

## The crystallography of three-flavor quark matter

Krishna Rajagopal<sup>1,2</sup>, and Rishi Sharma<sup>1,y</sup><sup>1</sup>Center for Theoretical Physics, Massachusetts Institute of Technology, Cambridge, MA 02139<sup>2</sup>Nuclear Science Division, MS 70R 319, Lawrence Berkeley National Laboratory, Berkeley, CA 94720

(Dated: March 26, 2022)

We analyze and compare candidate crystal structures for the crystalline color superconducting phase that may arise in cold, dense but not asymptotically dense, three-flavor quark matter. We determine the gap parameter and free energy ( ) for many possible crystal structures within a Ginzburg-Landau approximation, evaluating ( ) to order  $\mu^{-6}$ . In contrast to the two-flavor case, we find a positive  $\mu^6$  term and hence an ( ) that is bounded from below for all the structures that we analyze. This means that we are able to evaluate and as a function of the splitting between Fermi surfaces for all the structures we consider. We find two structures with particularly robust values of and the condensation energy, within a factor of two of those for the CFL phase which is known to characterize QCD at asymptotically large densities. The robustness of these phases results in their being favored over wide ranges of density. However, it also implies that the Ginzburg-Landau approximation is not quantitatively reliable. We develop qualitative insights into what makes a crystal structure favorable, and use these to winnow the possibilities. The two structures that we find to be most favorable are both built from condensates with face-centered cubic symmetry: in one case, the hdi and hsi condensates are separately face centered cubic; in the other case hdi and hsi combined make up a face centered cube.

PACS numbers: 12.38.-t, 26.60.+c, 12.38.Mh, 74.20.-z

## I. INTRODUCTION

Quantum chromodynamics predicts that at densities that are high enough that baryons are crushed into quark matter, the quark matter that results features pairing between quarks at low enough temperatures, meaning that it is in one of a family of possible color superconducting phases [1]. The essence of color superconductivity is quark pairing driven by the BCS mechanism, which operates whenever there are attractive interactions between fermions at a Fermi surface [2]. The interaction between quarks in QCD is strong and is attractive between quarks that are antisymmetric in color, so we expect cold dense quark matter to exhibit color superconductivity. If color superconducting quark matter occurs in nature, it lies within compact stars. Except during the first few seconds after their birth in supernovae, these stars have temperatures well below the tens of MeV. This implies that if these stars feature quark matter cores, these cores will be color superconductors, and justifies us in restricting our investigation

to  $T = 0$  throughout this paper.

We shall only consider Cooper pairs whose pair wave function is antisymmetric in Dirac indices | the relativistic generalization of zero total spin. (Other possibilities have been investigated [1, 3, 4, 5, 6] and found to be less favorable.) This in turn requires antisymmetry in flavor, meaning in particular that the two quarks in a Cooper pair must have different flavor.

It is by now well-established that at sufficiently high densities, where the up, down and strange quarks can be treated on an equal footing and the disruptive effects of the strange quark mass can be neglected, quark matter is in the color-flavor locked (CFL) phase, in which quarks of all three colors and all three flavors form conventional Cooper pairs with zero total momentum, and all fermionic excitations are gapped, with the gap parameter  $\sim 10-100$  MeV [1, 5]. However, even at the very center of a compact star the quark number chemical potential cannot be much larger than 500 MeV, meaning that the strange quark mass  $m_s$  (which is density dependent, lying somewhere between its vacuum current mass of about 100 MeV and constituent mass of about 500 MeV) cannot be neglected. Furthermore, bulk matter, as relevant for a compact star, must be in weak equilibrium and must be electrically and

---

Electronic address: krishna@lns.mit.edu<sup>y</sup>Electronic address: sharmaa@mit.edu

color neutral [6, 7, 8, 9, 10]. All these factors work to separate the Fermi momenta of the three different flavors of quarks, and thus disfavor the cross-species BCS pairing that characterizes the CFL phase. If we imagine beginning at asymptotically high densities and reducing the density, and suppose that CFL pairing is disrupted by the heaviness of the strange quark before color superconducting quark matter is superseded by baryonic matter, the CFL phase must be replaced by some phase of quark matter in which there is less, and less symmetric, pairing.

Within a spatially homogeneous ansatz, the next phase down in density is the gapless CFL (gCFL) phase [11, 12, 13, 14, 15, 16, 17, 18]. In this phase, quarks of all three colors and all three flavors still form ordinary Cooper pairs, with each pair having zero total momentum, but there are regions of momentum space in which certain quarks do not succeed in pairing, and these regions are bounded by momenta at which certain fermionic quasiparticles are gapless. This variation on BCS pairing—in which the same species of fermions that pair feature gapless quasiparticles—was first proposed for two-flavor quark matter [19] and in an atomic physics context [20]. In all these contexts, however, the gapless paired state turns out in general to suffer from a “magnetic instability”: it can lower its energy by the formation of counter-propagating currents [21, 22, 23]. In the atomic physics context, the resolution of the instability is phase separation, into macroscopic regions of two phases in one of which standard BCS pairing occurs and in the other of which no pairing occurs [24, 25, 26]. In three-flavor quark matter, where the instability of the gCFL phase has been established in Refs. [22], phase coexistence would require coexisting components with opposite color charges, in addition to opposite electric charges, making it very unlikely that a phase separated solution can have lower energy than the gCFL phase [12, 13]. Furthermore, color superconducting phases which are less symmetric than the CFL phase but still involve only conventional BCS pairing, for example the much-studied 2SC phase in which only two colors of up and down quarks pair [4, 27, 28] but including also many other possibilities [29], cannot be the resolution of the gCFL instability [6, 29]. It seems likely, therefore, that a ground state with counter-propagating currents is required. This could take the form of a crystalline color superconductor [30, 31, 32, 33, 34, 35, 36, 37, 38, 39, 40, 41]

the QCD analogue of a form of non-BCS pairing first considered by Larkin, Ovchinnikov, Fulde and Ferrell [42]. Or, given that the CFL phase itself is likely augmented by kaon condensation [43, 44], it could take the form of a phase in which a CFL kaon condensate carries a current in one direction balanced by a counter-propagating current in the opposite direction carried by gapless quark quasiparticles [45, 46]. This meson supercurrent phase has been shown to have a lower free energy than the gCFL phase.

Our purpose in this paper is to analyze and compare candidate crystal structures for three-flavor crystalline color superconductivity. The investigation of crystalline color superconductivity in three-flavor QCD was initiated in Ref. [39]. Although such phases seem to be free from magnetic instability [40], it remains to be seen whether such a phase can have a lower free energy than the meson current phase, making it a possible resolution to the gCFL instability. The simplest “crystal” structures do not suffice [39, 41], but experience in the two-flavor context [35] suggests that realistic crystal structures constructed from more plane waves will prove to be qualitatively more robust. Our results confirm this expectation.

Determining the favored crystal structure(s) in the crystalline color superconducting phase(s) of three-flavor QCD requires determining the gaps and comparing the free energies for very many candidate structures, as there are even more possibilities than the many that were investigated in the two-flavor context [35]. As there, we shall make a Ginzburg-Landau approximation. This approximation is controlled if  $\Delta_0 \ll \mu$ , where  $\Delta_0$  is the gap parameter of the crystalline color superconducting phase itself and  $\mu$  is the gap parameter in the CFL phase that would occur if  $M_s$  were zero. We shall find that the most favored crystal structures can have  $\Delta_0/\mu$  as large as  $\Delta_0/\mu = 1/2$ , meaning that we are pushing the approximation hard and so should not trust it quantitatively. In earlier work with Mannarelli [41], we analyzed a particularly simple one-parameter family of “crystal” structures in three-flavor quark matter, simple enough that we were able to do the analysis both with and without the Ginzburg-Landau approximation. We found that the approximation works when it should and that, at least for the simple crystal structures we analyzed in Ref. [41], when it breaks down it always underestimates the gap and the condensation energy. Furthermore, we found

that the Ginzburg-Landau approximation correctly determines which crystal structure among the one parameter family that we analyzed in Ref. [41] has the largest gap and lowest free energy.

We shall work throughout in a Nambu{Jona-Lasinio (NJL) model in which the QCD interaction between quarks is replaced by a point-like four-quark interaction, with the quantum numbers of single-gluon exchange, analyzed in mean field theory. This is not a controlled approximation. However, it suffices for our purposes: because this model has attraction in the same channels as in QCD, its high density phase is the CFL phase; and, the Fermi surface splitting effects whose qualitative consequences we wish to study can all be built into the model. Note that we shall assume throughout that  $\mu_0 = 0$ . This weak coupling assumption means that the pairing is dominated by modes near the Fermi surfaces. Quantitatively, this means that results for the gaps and condensation energies of candidate crystalline phases are independent of the cutoff in the NJL model when expressed in terms of the CFL gap  $\mu_0$ : if the cutoff is changed with the NJL coupling constant adjusted so that  $\mu_0$  stays fixed, the gaps and condensation energies for the candidate crystalline phases also stay fixed. This makes the NJL model valuable for making the comparisons that are our goal.

We shall consider crystal structures in which there are two condensates

$$\begin{aligned} \text{hudi} &= \sum_3^X \exp(2iq_3^a \cdot r) \\ \text{husi} &= \sum_2^X \exp(2iq_2^a \cdot r) : \end{aligned} \quad (1)$$

As in Refs. [39, 41], and as we explain in Section II, we neglect hdsi pairing because the d and s Fermi surfaces are twice as far apart from each other as each is from the intervening u Fermi surface. Were we to set  $\mu_2$  to zero, treating only hudi pairing, we would recover the two-avor Ginzburg-Landau analysis of Ref. [35]. There, it was found that the best choice of crystal structure was one in which pairing occurs for a set of eight  $q_3^a$ 's pointing at the corners of a cube in momentum space, yielding a condensate with face-centered cubic symmetry. The analyses of three-avor crystalline color superconductivity in Refs. [39, 41] introduce nonzero  $\mu_2$ , but made the simplifying ansatz that pairing occurs only for a single  $q_3$  and a single  $q_2$ . We consider crystal structures with up to eight  $q_3^a$ 's and up to eight  $q_2^a$ 's.

We shall evaluate the free energy  $\mathcal{F}(\mu_2; \mu_3)$  for each crystal structure, in a Ginzburg-Landau expansion in powers of the  $\mu$ 's. We work up to order  $\mu^{\frac{p}{2}} \mu^{\frac{q}{3}}$  with  $p+q=6$ . At sextic order, we find that  $\mathcal{F}(\mu_2; \mu_3)$  is positive for large  $\mu$  for all the crystal structures that we investigate. This is in marked contrast to the results of Ref. [35], which showed that many two-avor crystal structures have negative sextic terms, with free energies that are unbounded from below when the Ginzburg-Landau expansion is stopped at sextic order. Because we find positive sextic terms, we are able to use our sextic Ginzburg-Landau expansion to evaluate  $\mathcal{F}$  and  $\mathcal{F}'$  for all the structures that we analyze.

The two crystal structures that we argue are most favorable are both related to the face-centered cube of Ref. [35], but in different ways. In the first, which we denote "CubeX" in Section VI, there are four  $q_3^a$ 's and four  $q_2^a$ 's which together point at the eight corners of a cube in momentum space. In the second, denoted "2Cube45z" in Section VI, there are eight  $q_3^a$ 's and eight  $q_2^a$ 's which each point at the eight corners of a cube in momentum space, the two cubes rotated relative to each other by 45 degrees about an axis perpendicular to their faces. To a large degree, our argument that these two structures are the most favorable relies only on two qualitative inputs. First, if either the set of  $fq_2^a g$ 's or the set of  $fq_3^a g$ 's yields a hudi or a hdsi condensate whose free energy, viewed in isolation as a two-avor problem and evaluated as in Ref. [35], is unfavorable, then the three-avor condensate is unfavorable. Thus, we can use all the qualitative results of Ref. [35]. Second, the free energy of a candidate three-avor crystal structure becomes less favorable the closer any  $q_2^a$  comes to the antipodes of any  $q_3^a$ . This second result is foreshadowed in the results of Refs. [39, 41], and the results of Ref. [41] indicate that it is valid beyond the Ginzburg-Landau approximation. We shall see in Section VI that these two qualitative lessons are sufficient to winnow the space of candidate crystal structures down to the two that our calculational results, also described in Section VI, demonstrate are indeed the most favorable.

We find that several of the crystal structures that we consider have gap parameters that can be as large as  $\mu_0=3$ , and that one of them (the CubeX structure) has  $\mu = \mu_0$  that reaches 1/2. The robustness of these crystalline condensates thus pushes the Ginzburg-Landau approximation that we have used in the derivation of our results to the edge of its

regime of quantitative reliability. As we discussed above, the analysis of Ref. [41] shows that for simpler crystal structures qualitative results obtained within this approximation remain valid when the approximation has broken down quantitatively. We expect this to be so also for the more realistic, and complicated, crystal structures that we have constructed, but a demonstration would require their analysis without making a Ginzburg-Landau approximation, something we do not attempt here.

We find that the two crystal structures which we argue are most favorable have large condensation energies, easily  $1/3$  to  $1/2$  of that in the CFL phase with  $M_s = 0$ , which is  $3 \frac{2}{3} \mu^2 = \mu^2$ . This is remarkable, given the only quarks that pair are those lying on (admittedly many) rings on the Fermi surfaces, whereas in the CFL phase with  $M_s = 0$  pairing occurs over the entire  $u$ ,  $d$  and  $s$  Fermi surfaces.

The gapless CFL (gCFL) phase provides a useful comparison at nonzero  $M_s$ . For  $2 \mu_0 < M_s^2 < 5 \mu_0$ , model analyses that are restricted to isotropic phases predict a gCFL phase [11, 12, 15], finding this phase to have lower free energy than either the CFL phase or unpaired quark matter. However, this phase is unstable to the formation of current-carrying condensates [21, 22, 23, 45, 46] and so it cannot be the ground state. The true ground state must have lower free energy than that of the gCFL phase, and for this reason the gCFL free energy provides a useful benchmark. We find that three-flavor crystalline color superconducting quark matter has a lower free energy than both gCFL quark matter and unpaired quark matter within a wide regime of density. For

$$2.9 \mu_0 < \frac{M_s^2}{\mu_0} < 10.4 \mu_0 \quad (2)$$

the crystalline phase with one or other of the two crystal structures that we argue are most favorable has lower free energy (greater condensation energy) than CFL quark matter, gCFL quark matter, and unpaired quark matter. (See Fig. 7 in Section VI.) This window in parameter space is in no sense narrow. Our results therefore indicate that three-flavor crystalline quark matter will occur over a wide range of densities, unless, that is, the pairing between quarks is so strong (that is,  $\mu_0$  is so large making  $M_s^2 = \mu_0$  so small) that quark matter is in the CFL phase all the way down to the density at which quark matter is superseded by nuclear matter.

However, our results also indicate that unless the

Ginzburg-Landau approximation is underestimating the condensation energy of the crystalline phase by about a factor of two, there is a fraction of the "gCFL window" (with  $2 \mu_0 < M_s^2 < 2.9 \mu_0$ , in the Ginzburg-Landau approximation) in which no crystalline phase has lower free energy than the gCFL phase. This is thus the most likely regime in which to find the current-carrying meson condensates of Refs. [45, 46].

Our paper is organized as follows. In Section II, we shall specify the model we use and the simplifying assumptions we make, valid for  $\mu_0$ . Along the way we review relevant aspects of two-flavor color superconductivity. We shall also define our ansatz for the crystalline condensates more precisely than in Eq. (1). Much of Section II closely follows our earlier paper in collaboration with Mannarelli [41]. One simplifying assumption that we make is that  $\mu_2$  and  $\mu_3$  are equal in magnitude, an assumption which is related to how electric neutrality is maintained. In Appendix A, we use our results to confirm the validity of this assumption. In Section III we introduce the Ginzburg-Landau expansion of the free energy, deferring the derivation of the expressions for the Ginzburg-Landau coefficients to Section IV and their evaluation to Section V. We give our results in Section VI, and discuss their implications for future work in Section VII.

## II. MODEL, SIMPLIFICATIONS AND ANSATZ

### A. Neutral unpaired three-flavor quark matter

We shall analyze quark matter containing massless  $u$  and  $d$  quarks and  $s$  quarks with an effective mass  $M_s$ . (Although the strange quark mass can be determined self-consistently by solving for an chiral condensate [9, 17, 18], we shall leave this to future work and treat  $M_s$  as a parameter.) The Lagrangian density describing this system in the absence of interactions is given by

$$L_0 = \bar{\psi}_i \not{\partial} \psi_{ij} - \bar{\psi}_i M_{ij} \psi_j + \bar{\psi}_i \not{\partial} \psi_j; \quad (3)$$

where  $i, j = 1, 2, 3$  are flavor indices and  $\bar{\psi}_i = \bar{\psi}_{i\alpha}$  are color indices and we have suppressed the Dirac indices, where  $M_{ij} = \text{diag}(0, 0, M_s)_{ij}$  is the mass matrix, where  $\psi_{ij} = \psi_{i\alpha j}$  and where

the quark chemical potential matrix is given by

$$\mu_{ij} = (\mu_{ij}^e + Q_{ij}) + \mu_{ij}^3 T_3 + \frac{2}{3} \mu_{ij}^8 T_8 ; \quad (4)$$

with  $Q = \text{diag}(2/3; -1/3; -1/3)$ , the quark electric-charge matrix and  $T_3$  and  $T_8$  the Gell-Mann matrices in color space. We shall quote results at quark number chemical potential  $\mu = 500 \text{ MeV}$  throughout.

In QCD,  $\mu_e$ ,  $\mu_3$  and  $\mu_8$  are the zeroth components of electromagnetic and color gauge fields, and the gauge field dynamics ensure that they take on values such that the matter is neutral [6, 47], satisfying

$$\frac{\partial}{\partial \mu_e} = \frac{\partial}{\partial \mu_3} = \frac{\partial}{\partial \mu_8} = 0 ; \quad (5)$$

with the free energy density of the system. In the NJL model that we shall employ, in which quarks interact via four-fermion interactions and there are no gauge fields, we introduce  $\mu_e$ ,  $\mu_3$  and  $\mu_8$  by hand, and choose them to satisfy the neutrality constraints (5). The assumption of weak equilibrium is built into the calculation via the fact that the only flavor-dependent chemical potential is  $\mu_e$ , ensuring for example that the chemical potentials of d and s quarks with the same color must be equal. Because the strange quarks have greater mass, the equality of their chemical potentials implies that the s quarks have smaller Fermi momenta than the d quarks in the absence of BCS pairing. In the absence of pairing, then, because weak equilibrium drives the massive strange quarks to be less numerous than the down quarks, electrical neutrality requires a  $\mu_e > 0$ , which makes the up quarks less numerous than the down quarks and introduces some electrons into the system. In the absence of pairing, color neutrality is obtained with  $\mu_3 = \mu_8 = 0$ :

The Fermi momenta of the quarks and electrons in quark matter that is electrically and color neutral and in weak equilibrium are given in the absence of pairing by

$$\begin{aligned} p_F^d &= \sqrt{\frac{e}{3}} \\ p_F^u &= \sqrt{\frac{2e}{3}} \\ p_F^s &= \sqrt{\frac{e}{3} + \frac{e^2}{3} M_s^2} + \frac{e}{3} \frac{M_s^2}{2} \\ p_F^e &= \mu_e ; \end{aligned} \quad (6)$$

where we have simplified  $p_F^s$  upon assuming that  $M_s$  and  $\mu_e$  are small compared to  $\sqrt{e}$  by working only to

linear order in  $\mu_e$  and  $M_s^2$ . The free energy of the noninteracting quarks and electrons is given by

$$\begin{aligned} \text{unpaired} &= \frac{3 (p_F^u)^4 + 3 (p_F^d)^4 + (p_F^e)^4}{12 \pi^2} \\ &+ \frac{3}{2} \int_0^{p_F^s} p^2 dp \sqrt{p^2 + M_s^2} - \frac{e}{3} \\ &\frac{3}{4 \pi^2} \mu_e^4 - \frac{1}{2} M_s^2 \mu_e + \dots \end{aligned} \quad (7)$$

To this order, electric neutrality requires

$$\mu_e = \frac{M_s^2}{4} ; \quad (8)$$

yielding

$$\begin{aligned} p_F^d &= \sqrt{\frac{M_s^2}{12}} = p_F^u + \frac{M_s^2}{4} \\ p_F^u &= \sqrt{\frac{M_s^2}{6}} \\ p_F^s &= \sqrt{\frac{5M_s^2}{12}} = p_F^u + \frac{M_s^2}{4} \\ p_F^e &= \frac{M_s^2}{4} ; \end{aligned} \quad (9)$$

We see from (6) that to leading order in  $M_s^2$  and  $\mu_e$ , the effect of the strange quark mass on unpaired quark matter is as if instead one reduced the strange quark chemical potential by  $M_s^2/2$ . We shall make this approximation throughout. The corrections to this approximation in an NJL analysis of a two-flavor crystalline color superconductor have been evaluated and found to be small [34], and we expect the same to be true here. Upon making this assumption, we need no longer be careful about the distinction between  $p_F$ 's and  $\mu$ 's, as we can simply think of the three flavors of quarks as if they have chemical potentials

$$\begin{aligned} \mu_d &= \mu_u + 2 \mu_3 \\ \mu_u &= \mu_F^u \\ \mu_s &= \mu_u - 2 \mu_2 \end{aligned} \quad (10)$$

with

$$\mu_3 = \mu_2 = \frac{M_s^2}{8} ; \quad (11)$$



where the choice of subscripts indicates that  $2_{23}$  is the splitting between the Fermi surfaces for quarks 1 and 3 and  $2_{13}$  is that between the Fermi surfaces for quarks 1 and 2, identifying  $u;d;s$  with  $1;2;3$ . (The prefactor 2 in the equations defining the  $\mu$ 's is chosen to agree with the notation used in the analysis of crystalline color superconductivity in a two flavor model [30], in which the two Fermi surfaces were denoted by  $\mu_1$  meaning that they were separated by  $2\mu_1$ .)

Note that the equality of  $2_{23}$  and  $2_{13}$  is only valid to leading order in  $M_s^2$ ; at the next order,  $\mu_e = M_s^2 = (4\pi)^{-1} M_s^4 = (48\pi)^{-3}$  and  $\mu_3 = \mu_e = 2$  while  $\mu_2 = \mu_3 + M_s^4 = (16\pi)^{-3}$ . In Section V, we will utilize the fact that  $2_{23}$  and  $2_{13}$  are close to equal, but not precisely equal.

### B. BCS pairing and neutrality

As described in Refs. [6, 9, 11, 48], BCS pairing introduces qualitative changes into the analysis of neutrality. For example, in the CFL phase  $\mu_e = 0$  and  $\mu_8$  is nonzero and of order  $M_s^2$ . This arises because the construction of a phase in which BCS pairing occurs between fermions whose Fermi surface would be split in the absence of pairing can be described as follows. First, adjust the Fermi surfaces of those fermions that pair to make them equal. This costs a free energy price of order  $\mu^2$ . And, it changes the relation between the chemical potentials and the particle numbers, meaning that the  $\mu$ 's required for neutrality can change qualitatively as happens in the CFL example. Second, pair. This yields a free energy benefit of order  $\mu_0^2$ , where  $\mu_0$  is the gap parameter describing the BCS pairing. Hence, BCS pairing will only occur if the attraction between the fermions is large enough that  $\mu_0 \gg \mu$ . In the CFL context, in which  $h_{ud}$ ,  $h_{us}$  and  $h_{ds}$  pairing is fighting against the splitting between the  $d$ ,  $u$  and  $s$  Fermi surfaces described above, it turns out that CFL pairing can occur if  $\mu_0 > 4\mu = M_s^2 = (2\pi)^{-1}$  [11], a criterion that is reduced somewhat by kaon condensation which acts to stabilize CFL pairing [44].

In this paper we are considering quark matter at densities that are low enough ( $\mu < M_s^2 = (2\pi)^{-1}$ ) that CFL pairing is not possible. The gap parameter  $\mu_0$  that would characterize the CFL phase if  $M_s^2$  and  $\mu$  were zero is nevertheless an important scale in our problem, as it quantifies the strength of the attraction between quarks. Estimates of the magnitude of

$\mu_0$  are typically in the tens of MeV, perhaps as large as 100 MeV [1]. We shall treat  $\mu_0$  as a parameter, and quote results for  $\mu_0 = 25$  MeV, although as we shall show in Section VI E our results can easily be scaled to any value of  $\mu_0$  as long as the weak-coupling approximation  $\mu_0 \gg \mu$  is respected.

### C. Crystalline color superconductivity in two-flavor quark matter

Crystalline color superconductivity can be thought of as the answer to the question: "Is there a way to pair quarks at differing Fermi surfaces without first equalizing their Fermi momenta, given that doing so exacts a cost?" The answer is "Yes, but it requires Cooper pairs with nonzero total momentum." Ordinary BCS pairing pairs quarks with momenta  $p$  and  $-p$ , meaning that if the Fermi surfaces are split at most one member of a pair can be at its Fermi surface. In the crystalline color superconducting phase, pairs with total momentum  $2q$  condense, meaning that one member of the pair has momentum  $p + q$  and the other has momentum  $-p + q$  for some  $p$  [30, 42]. Suppose for a moment that only  $u$  and  $d$  quarks pair, making the analyses of a two-flavor model found in Refs. [30, 31, 32, 33, 34, 35, 36, 37, 38] (and really going back to Ref. [42]) valid. We sketch the results of this analysis in this subsection.

The simplest "crystalline" phase is one in which only pairs with a single  $q$  condense, yielding a condensate

$$h_u(x)C_{sd}(x)i / \exp(2iq \cdot r) \quad (12)$$

that is modulated in space like a plane wave. (Here and throughout, we shall denote by  $r$  the spatial three-vector corresponding to the Lorentz four-vector  $x$ .) Assuming that  $\mu_0 \gg \mu$ , the energetically favored value of  $|q|$  turns out to be  $q = \mu_0/2$ , where the proportionality constant is given by  $\mu_0 = 1.1997 \mu_0$  [30, 42]. If  $\mu_0$  were 1, then the only choice of  $p$  for which a Cooper pair with momenta  $(p + q; -p + q)$  would describe two quarks each on their respective Fermi surfaces would correspond to a quark on the north pole of one Fermi surface and a quark on the south pole of the other. Instead, with  $\mu_0 > 1$ , the quarks on each Fermi surface that can pair lie on one ring on each Fermi surface, the rings having opening angle  $\theta_0 = 2 \cos^{-1}(1/\mu_0) = 67.1^\circ$ . The energetic calculation that determines  $\mu_0$  can be

thought of as balancing the gain in pairing energy as  $\mu$  is increased beyond 1, allowing quarks on larger rings to pair, against the kinetic energy cost of Cooper pairs with greater total momentum. If the  $\mu = 0$  Ginzburg-Landau limit is not assumed, the pairing rings change from circular lines on the Fermi surfaces into ribbons of thickness  $\Delta$  and angular extent  $\Delta/\mu$ . The condensate (12) carries a current, which is balanced by a counter-propagating current carried by the unpaired quarks near their Fermi surfaces that are not in the pairing ribbons. Hence, the state carries no net current.

After solving a gap equation for  $\Delta$  and then evaluating the free energy of the phase with condensate (12), one finds that this simplest "crystalline" phase is favored over two-avor quark matter with either no pairing or BCS pairing only within a narrow window

$$0.707 \mu_{2SC} < \mu < 0.754 \mu_{2SC}; \quad (13)$$

where  $\mu_{2SC}$  is the gap parameter for the two-avor phase with 2SC (2-avor, 2-color) BCS pairing found at  $\mu = 0$ . At the upper boundary of this window,

$\mu = 0$  and one finds a second order phase transition between the crystalline and unpaired phases. At the lower boundary, there is a first order transition between the crystalline and BCS paired phases. The crystalline phase persists in the weak coupling limit only if  $\mu = \mu_{2SC}$  is held fixed, within the window (13), while the standard weak-coupling limit  $\mu_{2SC} = 0$  is taken. Looking ahead to our context, and recalling that in three-avor quark matter  $\mu_s^2 = M_s^2/8$ , we see that at high densities one finds the CFL phase (which is the three-avor quark matter BCS phase) and in some window of lower densities one finds a crystalline phase. In the vicinity of the second order transition, where  $\mu = 0$  and in particular where  $\mu = 0$  and, consequently given (13),  $\mu = \mu_{2SC} = 0$  a Ginzburg-Landau expansion of the free energy order by order in powers of  $\mu$  is controlled. A analysis within an NJL model shows that the results for (13) become accurate in the limit  $\mu \rightarrow 0.754 \mu_{2SC}$  where  $\mu = 0$ , as must be the case, and show that the Ginzburg-Landau approximation underestimates (13) at all  $\mu$  [30, 35].

The Ginzburg-Landau analysis can then be applied to more complicated crystal structures in which Cooper pairs with several different  $q$ 's, all with the same length but pointing in different directions, arise [35]. This analysis indicates that a face-centered cubic structure constructed as the sum of

eight plane waves with  $q$ 's pointing at the corners of a cube is favored, but it does not permit a quantitative evaluation of (13). The Ginzburg-Landau expansion of the free energy has terms that are quartic and sextic in  $\Delta$  whose coefficients are both large in magnitude and negative. To this order, is not bounded from below. This means that the Ginzburg-Landau analysis predicts a strong first order phase transition between the crystalline and unpaired phase, at some  $\mu$  significantly larger than  $0.754 \mu_{2SC}$ , meaning that the crystalline phase occurs over a range of  $\mu$  that is much wider than (13), but it precludes the quantitative evaluation of the  $\mu$  at which the transition occurs, of  $\mu_{2SC}$ , or of  $\mu$ .

We shall find that in three-avor quark matter, all the crystalline phases that we analyze have Ginzburg-Landau free energies with positive sextic coefficient, meaning that they can be used to evaluate  $\mu$ , and the location of the transition from unpaired quark matter to the crystalline phase with a postulated crystal structure. For the most favored crystal structures, we find that the window in parameter space in which they occur is given by (2), which is in no sense narrow.

#### D. Crystalline color superconductivity in neutral three-avor quark matter

Our purpose in this paper is to analyze three-avor crystalline color superconductivity, with condensates as in Eq. (1) for a variety of choices of the sets of  $q_2^a$ 's and  $q_3^a$ 's, i.e. for a variety of crystal structures. We shall make weak coupling (namely  $\mu \rightarrow 0$ ;  $\Delta \rightarrow \infty$ ) and Ginzburg-Landau (namely  $\mu \rightarrow 0$ ;  $\Delta \rightarrow \infty$ ) approximations throughout.

The analysis of neutrality in three-avor quark matter in a crystalline color superconducting phase is very simple in the Ginzburg-Landau limit in which  $\mu = 0$ : because the construction of this phase does not involve rearranging any Fermi momenta prior to pairing, and because the assumption  $\mu = 0$  implies that the pairing does not significantly change any number densities, neutrality is achieved with the same chemical potentials  $\mu_s = M_s^2/8 = 0$  and  $\mu_3 = \mu_8 = 0$  as in unpaired quark matter, and with Fermi momenta given in Eqs. (6), (9), and (10) as in unpaired quark matter. This result is correct only in the Ginzburg-Landau limit.

We consider a condensate of the form

$$\chi_{ij}(\mathbf{x}) = \sum_{\mathbf{I}=1}^3 \sum_{\mathbf{q}_I^a} e^{2i\mathbf{q}_I^a \cdot \mathbf{r}_I} \chi_{ij}^{\mathbf{I}}; \quad (14)$$

where  $\mathbf{q}_1^a$ ,  $\mathbf{q}_2^a$  and  $\mathbf{q}_3^a$  and  $\chi_1$ ,  $\chi_2$  and  $\chi_3$  are the wave vectors and gap parameters describing pairing between the (d;s), (u;s) and (u;d) quarks respectively, whose Fermi momenta are split by  $2\chi_1$ ,  $2\chi_2$  and  $2\chi_3$  respectively. From (10), we see that  $\chi_2 = \chi_3 = \chi_1/2 = M_s^2/8$ . For each  $\mathbf{I}$ ,  $\mathbf{q}_I^a$  is a set of momentum vectors that define the periodic spatial modulation of the crystalline condensate describing pairing between the quarks whose flavor is not  $\mathbf{I}$ , and whose color is not  $\mathbf{I}$ . Our goal in this paper is to compare condensates with different choices of  $\mathbf{q}_I^a$ 's, that is with different crystal structures. To shorten expressions, we will henceforth write

$$\sum_{\mathbf{q}_I^a} e^{2i\mathbf{q}_I^a \cdot \mathbf{r}_I} : \quad (15)$$

The condensate (14) has the color-flavor structure of the CFL condensate (obtained by setting all  $\mathbf{q}$ 's to zero) and is the natural generalization to nontrivial crystal structures of the condensate previously analyzed in Refs. [39, 41], in which each  $\mathbf{q}_I^a$  contained only a single vector.

In the derivation of the Ginzburg-Landau approximation in Section IV, we shall make no further assumptions. However, in Sections V and VI when we evaluate the Ginzburg-Landau coefficients and give our results, we shall make the further simplifying assumption that  $\chi_1 = 0$ . Given that  $\chi_1$  is twice  $\chi_2$  or  $\chi_3$ , it seems reasonable that  $\chi_1 \gg \chi_2, \chi_3$ . We leave a quantitative investigation of condensates with  $\chi_1 \neq 0$  to future work.

#### E. NJL Model, and Mean-Field Approximation

As discussed in Section I, we shall work in an NJL model in which the quarks interact via a point-like four-quark interaction, with the quantum numbers of single-gluon exchange, analyzed in mean-field theory. By this we mean that the interaction term added to the Lagrangian (3) is

$$\mathcal{L}_{\text{interaction}} = \frac{3}{8} (\bar{\psi}^A \psi)(\bar{\psi}^A \psi); \quad (16)$$

where we have suppressed the color and flavor indices that we showed explicitly in (3), and have continued to suppress the Dirac indices. The full expression for  $\bar{\psi}^A \psi$  is  $(\bar{\psi}^A)_i \psi_j = (\bar{\psi}^A)_{ij}$ , where the  $T^A$  are the color Gell-Mann matrices. The NJL coupling constant has dimension  $-2$ , meaning that an ultraviolet cutoff must be introduced as a second parameter in order to fully specify the interaction. Defining as the restriction that momentum integrals be restricted to a shell around the Fermi surface,  $\langle \mathbf{p} | \mathbf{p} \rangle = \Lambda^3$ , the CFL gap parameter can then be evaluated: [1, 35]

$$\Delta_0 = 2^{\frac{2}{3}} \exp \left( -\frac{\Lambda^2}{2\mu^2} \right); \quad (17)$$

We shall see in subsequent sections that in the limit in which  $\Lambda \rightarrow 0$ , all our results can be expressed in terms of  $\Delta_0$ ; neither  $\Lambda$  nor  $\mu$  shall appear. This reflects the fact that in this limit the physics of interest is dominated by quarks near the Fermi surfaces, not near  $\mu$ , and so once  $\Delta_0$  is used as the parameter describing the strength of the attraction between quarks,  $\mu$  is no longer visible; the cutoff  $\Lambda$  only appears in the relation between  $\Delta_0$  and  $\mu$ , not in any comparison among different possible paired phases. In our numerical evaluations in Section VI, we shall take  $\mu = 500 \text{ MeV}$ ,  $\Lambda = 100 \text{ MeV}$ , and adjust  $\Delta_0$  to be such that  $\Delta_0$  is  $25 \text{ MeV}$ .

In the mean-field approximation, the interaction Lagrangian (16) takes on the form

$$\mathcal{L}_{\text{interaction}} = \frac{1}{2} (\bar{\chi})^T + \frac{1}{2} \chi^T; \quad (18)$$

where  $\chi(\mathbf{x})$  is related to the diquark condensate by the relations

$$\begin{aligned} \chi(\mathbf{x}) &= \frac{3}{4} \bar{\psi}^A \psi^T (\bar{\psi}^A)^T \\ \chi(\mathbf{x}) &= \frac{3}{4} (\bar{\psi}^A)^T \psi^T \bar{\psi}^A \\ &= \bar{\psi}^0 \psi^0(\mathbf{x}) \bar{\psi}^0; \end{aligned} \quad (19)$$

The ansatz (14) can now be made precise: we take

$$\chi(\mathbf{x}) = C_F \chi(\mathbf{x}) C^{-5}; \quad (20)$$

with

$$C_F \chi(\mathbf{x})_{ij} = \sum_{\mathbf{I}=1}^3 \sum_{\mathbf{q}_I^a} (\bar{\psi}^a_I) e^{2i\mathbf{q}_I^a \cdot \mathbf{r}_I} \chi_{ij}^{\mathbf{I}}; \quad (21)$$



We have introduced notation that allows for the possibility of gap parameters  $(q_I^a)$  with different magnitudes for different  $I$  and for different  $a$ . In fact, we shall only consider circumstances in which  $(q_I^a) = \delta_{aI}$ , as in (14). However, it will be very convenient in subsequent sections to keep track of which  $I$  in a complicated equation "goes with" which  $q_I^a$ , making this notation useful.

The full Lagrangian, given by the sum of (3) and (18), is then quadratic and can be written very simply upon introducing the two component Nambu-Gorkov spinor

$$\Psi = \begin{pmatrix} \psi \\ \psi^\dagger \end{pmatrix} \quad \text{and hence} \quad \bar{\Psi} = \begin{pmatrix} \bar{\psi} & \bar{\psi}^\dagger \end{pmatrix}; \quad (22)$$

in terms of which

$$L = \frac{1}{2} \bar{\Psi} \begin{pmatrix} i\partial_t + \mathbf{p} \cdot \mathbf{v} & \mathbf{p} \cdot \mathbf{v} \\ \mathbf{p} \cdot \mathbf{v} & i\partial_t - \mathbf{p} \cdot \mathbf{v} \end{pmatrix} \Psi; \quad (23)$$

Here,  $\mathbf{v} = \mathbf{v}_0$  and  $\mathbf{v}$  is the matrix (4), which we have argued simplifies to

$$\mathbf{v} = \text{diag}(\mathbf{v}_u; \mathbf{v}_d; \mathbf{v}_s) \quad (24)$$

with the flavor chemical potentials given simply by (10). In subsequent sections, we shall also often use the notation  $\Psi_i = \Psi_{i0}$ , with  $i = 1, 2, 3$  corresponding to  $u; d; s$  respectively.

The propagator corresponding to the Lagrangian (23) is given by

$$\begin{aligned} \langle \Psi(x) \bar{\Psi}(x^0) \rangle &= \begin{pmatrix} \langle \psi(x) \bar{\psi}(x^0) \rangle & \langle \psi(x) \bar{\psi}^\dagger(x^0) \rangle \\ \langle \psi^\dagger(x) \bar{\psi}(x^0) \rangle & \langle \psi^\dagger(x) \bar{\psi}^\dagger(x^0) \rangle \end{pmatrix} \\ &= \begin{pmatrix} iG(x; x^0) & iF(x; x^0) \\ iF(x; x^0) & iG(x; x^0) \end{pmatrix}; \end{aligned} \quad (25)$$

where  $G$  and  $G$  are the "normal" components of the propagator and  $F$  and  $F$  are the "anomalous" components. They satisfy the coupled differential equations

$$\begin{aligned} i\partial_t \begin{pmatrix} \psi \\ \psi^\dagger \end{pmatrix} &= \begin{pmatrix} x & \\ & x \end{pmatrix} \begin{pmatrix} G(x; x^0) & F(x; x^0) \\ F(x; x^0) & G(x; x^0) \end{pmatrix} \begin{pmatrix} \psi \\ \psi^\dagger \end{pmatrix} \\ &= \begin{pmatrix} 1 & 0 \\ 0 & 1 \end{pmatrix} \begin{pmatrix} 0 & \\ & 0 \end{pmatrix} \begin{pmatrix} \psi \\ \psi^\dagger \end{pmatrix}; \end{aligned} \quad (26)$$

We can now rewrite (19) as

$$\begin{aligned} \psi(x) &= \frac{3i}{4} \mathbf{A}^T F(x; x) (\mathbf{A})^T \\ \psi^\dagger(x) &= \frac{3i}{4} (\mathbf{A})^T F(x; x) \mathbf{A}; \end{aligned} \quad (27)$$

either one of which is the self-consistency equation, or gap equation, that we must solve. Without further approximation, (27) is not tractable. It yields an infinite set of coupled gap equations, one for each  $(q_I^a)$ , because without further approximation it is not consistent to choose finite sets  $f_{q_I^a}$ . When several plane waves are present in the condensate, they induce an infinite tower of higher momentum condensates [35]. The reason why the Ginzburg-Landau approximation, to which we now turn, is such a simplification is that it eliminates these higher harmonics.

### III. GINZBURG-LANDAU APPROXIMATION: INTRODUCTION

The form of the Ginzburg-Landau expansion of the free energy can be derived using only general arguments. This, combined with results for two-flavor crystalline color superconductivity from Ref. [35], will allow us to draw some partial conclusions in this Section.

We shall only consider crystal structures in which all the vectors  $q_I^a$  in the crystal structure  $f_{q_I^a}$  are "equivalent". By this we mean that a rigid rotation of the crystal structure can be found which maps any  $q_I^a$  to any other  $q_I^b$  leaving the set  $f_{q_I^a}$  invariant. For such crystal structures,  $(q_I^a) = \delta_{aI}$ , meaning that the free energy is a function only of  $\mu_1, \mu_2$  and  $\mu_3$ . As explained in Section IID, the chemical potentials that maintain neutrality in three-flavor crystalline color superconducting quark matter are the same as those in neutral unpaired three-flavor quark matter. Therefore,

$$\mu_{\text{crystalline}} = \mu_{\text{unpaired}} + (\mu_1; \mu_2; \mu_3); \quad (28)$$

with  $\mu_{\text{unpaired}}$  given in (7) with (8), and with  $(0; 0; 0) = 0$ . Our task is to evaluate the condensation energy  $(\mu_1; \mu_2; \mu_3)$ . Since our Lagrangian is baryon number conserving and contains no weak interactions, it is invariant under a global  $U(1)$  symmetry for each flavor. This means that  $\mu$  must be invariant under  $U(1) \ni e^{i\theta} U(1)$  for each  $I$ , meaning that each of the three  $\mu_I$ 's can only appear in the combination  $\mu_I - \mu$ . (Of course, the ground state can and does break these  $U(1)$  symmetries spontaneously; what we need in the argument we are making here is only that they are not explicitly broken in the Lagrangian.) We conclude that if we expand

( $\epsilon_I; \epsilon_J; \epsilon_K$ ) in powers of the  $\epsilon_I$ 's up to sextic order, it must take the form

$$\begin{aligned}
 (f_I g) = & \frac{2^{\frac{1}{2}}}{2} \sum_I P_I \epsilon_I^2 + \frac{1}{2} \sum_I \epsilon_I^4 + \frac{1}{3} \sum_I \epsilon_I^6 + \sum_{I>J} \epsilon_I^2 \epsilon_J^2 + \sum_{I>J>K} \epsilon_I^2 \epsilon_J^2 \epsilon_K^2 + \dots \\
 & + \sum_{I>J>K} \epsilon_I^2 \epsilon_J^2 \epsilon_K^2 + \dots
 \end{aligned} \tag{29}$$

where we have made various notational choices for later convenience. The overall prefactor of  $2^{\frac{1}{2}} = 2$  is the density of states at the Fermi surface of unpaired quark matter with  $M_s = 0$ ; it will prove convenient that we have defined all the coefficients in the Ginzburg-Landau expansion of the free energy relative to this. We have defined  $P_I = \dim f_{q_I} g$ , the number of plane waves in the crystal structure for the condensate describing pairing between quarks whose flavor and color are not  $I$ . Writing the prefactor  $P_I$  multiplying the quadratic term and writing the factors of  $\frac{1}{2}$  and  $\frac{1}{3}$  multiplying the quartic and sextic terms ensures that the  $\epsilon_I$ ,  $\epsilon_I$  and  $\epsilon_I$  coefficients are defined the same way as in Ref. [35]. The form of the Ginzburg-Landau expansion (29) is model independent, whereas the expressions for the coefficients  $P_I$ ,  $\epsilon_I$ ,  $\epsilon_J$ ,  $\epsilon_K$ ,  $\epsilon_I \epsilon_J$  and  $\epsilon_{123}$  for a given ansatz for the crystal structure are model-dependent. In Section IV we shall derive the Ginzburg-Landau approximation to our model, yielding expressions for these coefficients which we then evaluate in Section V.

We see in Eq. (29) that there are some coefficients — namely  $\epsilon_I$ ,  $\epsilon_I$  and  $\epsilon_I$  — which multiply polynomials involving only a single  $\epsilon_I$ . Suppose that we keep a single  $\epsilon_I$  nonzero, setting the other two to zero. This reduces the problem to one with two-flavor pairing only, and the Ginzburg-Landau coefficients for this problem have been calculated for many different crystal structures in Ref. [35]. We can then immediately use these coefficients, called  $\epsilon_I$ ,  $\epsilon_I$  and  $\epsilon_I$  in Ref. [35], to determine our  $\epsilon_I$ ,  $\epsilon_I$  and

$\epsilon_I$ . Using  $\epsilon_I$  as an example, we conclude that

$$\begin{aligned}
 \epsilon_I = (q_I; \epsilon_I) = & 1 + \frac{\epsilon_I}{2q_I} \log \frac{q_I + \epsilon_I}{q_I - \epsilon_I} \\
 & - \frac{1}{2} \log \frac{2^{2SC}}{4(q_I^2 - \epsilon_I^2)};
 \end{aligned} \tag{30}$$

where  $\epsilon_I$  is the splitting between the Fermi surfaces of the quarks with the two flavors other than  $I$  and  $q_I = |\mathbf{q}_I|$  is the length of the  $q$ -vectors in the set  $f_{q_I} g$ . (We shall see momentarily why all have the same length.) In (30),  $2SC$  is the gap parameter in the BCS state obtained with  $\epsilon_I = 0$  and  $\epsilon_I$  nonzero with the other two gap parameters set to zero. Assuming that  $\epsilon_0 > 0$ , this gap parameter for  $2SC$  (2-flavor, 2-color) BCS pairing is given by [1, 49]

$$2SC = 2^{\frac{1}{3}} \epsilon_0; \tag{31}$$

For a given  $\epsilon_I$  and  $\epsilon_0$ ,  $\epsilon_I$  given in (30) is minimized when [30, 35, 42]

$$q_I = \epsilon_I \text{ with } \epsilon_I = 1:1997; \tag{32}$$

In the Ginzburg-Landau approximation, in which the  $\epsilon_I$  are assumed to be small, we must first minimize the quadratic contribution to the free energy, before proceeding to investigate the consequences of the quartic and sextic contributions. Minimizing  $\epsilon_I$  fixes the length of all the  $q$ -vectors in the set  $f_{q_I} g$ , thus eliminating the possibility of higher harmonics. It is helpful to imagine the (three) sets  $f_{q_I} g$  as representing the vertices of (three) polyhedra in momentum space. By minimizing  $\epsilon_I$ , we have learned that each polyhedron  $f_{q_I} g$  can be inscribed

in a sphere of radius  $r_I$ . From the quadratic contribution to the free energy, we do not learn anything about what shape polyhedra are preferable. In fact, the quadratic analysis in isolation would indicate that if  $r_I < 0$  (which happens for  $r_I < 0.754 r_{2SC}$ ) then modes with arbitrarily many different  $q_I$ 's should condense. It is the quartic and sextic coefficients that describe the interaction among the modes, and hence control what shape polyhedra are in fact preferable.

The quartic and sextic coefficients  $r_I$  and  $r_{II}$  can also be taken directly from the two-avor results of Ref. [35]. They are given by  $r_I = \frac{2}{3}$  and  $r_{II} = \frac{4}{3}$  where  $r_I$  and  $r_{II}$  are dimensionless quantities depending only on the directions of the vectors in the set  $fq_I g$ . They have been evaluated for many crystal structures in Ref. [35], resulting in two qualitative conclusions. Recall that, as reviewed in Section II C, the presence of a condensate with some  $q_I^a$  corresponds to pairing on a ring on each Fermi surface with opening angle  $67.1^\circ$ . The first qualitative conclusion is that any crystal structure in which there are two  $q_I^a$ 's whose pairing rings intersect has very large, positive, values of both  $r_I$  and  $r_{II}$ , meaning that it is strongly disfavored. The second conclusion is that regular structures, those in which there are many ways of adding four or six  $q_I^a$ 's to form closed figures in momentum space, are favored. Consequently, according to Ref. [35] the favored crystal structure in the two-avor case has 8  $q_I^a$ 's pointing towards the corners of a cube. Choosing the polyhedron in momentum space to be a cube yields a face-centered cubic modulation of the condensate in position space.

Because the  $r_I$  and  $r_{II}$  coefficients in our problem can be taken over directly from the two-avor analysis, we can expect that it will be unfavorable for any of the three sets  $fq_I g$  to have more than eight vectors, or to have any vectors closer together than  $67.1^\circ$ . At this point we cannot exclude the possibility that the large positive  $r_I$  and  $r_{II}$  indicating an unfavorable  $fq_I g$  could be offset by large negative values for the other coefficients which we cannot read off from the two-avor analysis. However, what we shall instead find in Section VI is that  $r_{IJ}$  and  $r_{IIJ}$  are positive in all cases that we have investigated. This means that we know of no exceptions to the rule that if a particular  $fq_I g$  is unfavorable as a two-avor crystal structure, then any three-avor condensate in which this set of  $q$ -vectors describes either the  $1$ ,  $2$  or  $3$  crystal structure is also disfavored.

In Section IV we shall use our microscopic model to derive expressions for all the coefficients in the Ginzburg-Landau expansion (29), including rederiving those which we have taken above from the two-avor analysis of Ref. [35]. The coefficients that we cannot simply read off from a two-avor analysis are those that multiply terms involving more than one  $q_I$  and hence describe the interaction between the three different  $q_I$ 's. Before evaluating the expressions for the coefficients in Section V, we shall make the further simplifying assumption that  $r_1 = 0$ , because the separation  $r_1$  between the d and s Fermi surfaces is twice as large as that between either and the intervening u Fermi surface. This simplifies (29) considerably, eliminating the  $123$  term and all the  $r_{IJ}$  and  $r_{IIJ}$  terms except  $32$ ,  $223$  and  $332$ .

#### IV. THE GINZBURG-LANDAU APPROXIMATION: DERIVATION

We now derive the Ginzburg-Landau approximation to the NJL model specified in Section II. We proceed by first making a Ginzburg-Landau approximation to the gap equation, and then formally integrate the gap equation in order to obtain the free energy, since the gap equation is the variation of the free energy with respect to the gap parameters.

The gap equation (27) with which we closed Section II is an infinite set of coupled equations, one for each  $(q_I^a)$ , with each equation containing arbitrarily high powers of the  $q_I$ 's. In order to make a Ginzburg-Landau expansion, order by order in powers of the  $q_I$ 's, we first integrate (26), obtaining

$$\begin{aligned} G(x; x^0) &= G^{(0)}(x; x^0) - \int_Z d^4 z G^{(0)}(x; z) (z) F(z; x^0) \\ F(x; x^0) &= \int_Z d^4 z G^{(0)}(x; z) (z) G(z; x^0) \end{aligned} \quad (33)$$

with  $G^{(0)} = (i\epsilon + \gamma)^{-1}$  and  $G^{(0)} = ((i\epsilon - \gamma)^{-1})^{\dagger}$ . We then expand these equations order by order in  $(x)$  by iterating them. To fifth order, for  $F$  we find

$$\begin{aligned} F = & G^{(0)} G^{(0)} G^{(0)} G^{(0)} G^{(0)} G^{(0)} \\ & G^{(0)} G^{(0)} G^{(0)} G^{(0)} G^{(0)} G^{(0)} + O(\gamma^7); \end{aligned} \quad (34)$$

where we have suppressed space-time coordinates and integrals for simplicity. We then substitute this

$$\begin{aligned}
& \text{---} \Delta^\dagger \text{---} = -i\frac{3\lambda}{4} \left( -\frac{2}{3} \delta_{\alpha\alpha'} \delta_{\beta\beta'} + 2\delta_{\alpha\beta'} \delta_{\alpha'\beta} \right) \gamma^\mu \left[ \text{---} \Delta^\dagger \text{---} \right]_{\alpha i \beta j} \\
& + \text{---} \Delta^\dagger \text{---} \Delta \text{---} \Delta^\dagger \text{---} \Delta \text{---} + \text{---} \Delta^\dagger \text{---} \Delta \text{---} \Delta^\dagger \text{---} \Delta \text{---} \Delta \text{---} \Delta^\dagger \text{---} + \dots \gamma^\mu
\end{aligned}$$

FIG. 1: The gap equation. The labels  $\alpha, \beta$  represent the external color indices and  $i, j$  represent the external flavor indices. All the other color-flavor indices are contracted.  $C_F$  (and  $\bar{C}_F$ ) are matrices of the form (21) and carry the same color and flavor indices as the neighbouring propagators. The dashed lines represent the propagator  $(i\partial\!\!\!/ + m)^{-1}$  and the solid lines represent  $(i\partial\!\!\!/ + m)^{-1}$ . Evaluating the gap equation involves substituting (21) for  $C_F$ , doing the contraction over the internal color-flavor indices, and evaluating the loop integrals in momentum space.

expansion for  $F$  into the right-hand side of the gap equation for  $\chi$  in (27). After using the  $C_5$  Dirac structure of our ansatz (20) and the identity  $C(\gamma)^T C^{-1} = \gamma$  to simplify the expression, we

obtain the gap equation satisfied by  $C_F(\mathbf{x})$ , the part of our ansatz (20,21) that describes the color, flavor and spatial form of our condensate. To order  $\epsilon^5$ , we find

$$\begin{aligned}
\bar{C}_F &= \frac{3i}{4} (\bar{t}^a)^T \frac{h}{i\partial\!\!\!/ + m} = \bar{C}_F \frac{1}{i\partial\!\!\!/ + m} \\
&+ \frac{1}{i\partial\!\!\!/ + m} = \bar{C}_F \frac{1}{i\partial\!\!\!/ + m} = C_F \frac{1}{i\partial\!\!\!/ + m} = \bar{C}_F \frac{1}{i\partial\!\!\!/ + m} \\
&+ \frac{1}{i\partial\!\!\!/ + m} = \bar{C}_F \frac{1}{i\partial\!\!\!/ + m} = C_F \frac{1}{i\partial\!\!\!/ + m} = \bar{C}_F \frac{1}{i\partial\!\!\!/ + m} = C_F \frac{1}{i\partial\!\!\!/ + m} = \bar{C}_F \frac{1}{i\partial\!\!\!/ + m} = \frac{i}{(\mathbf{x}; \mathbf{x})} \bar{t}^a;
\end{aligned} \tag{35}$$

where the differential operators act on everything to their right and where we have continued to simplify the notation by not writing the space-time, color and flavor arguments of the  $C_F$ 's and by not writing the integrals. We then use the color Fierz identity

$$(\bar{t}^a)_{ij} (\bar{t}^a)_{kl} = \frac{2}{3} \delta_{ij} \delta_{kl} + 2 \delta_{il} \delta_{kj} \tag{36}$$

to rewrite (35) as shown diagrammatically in Fig. 1.

As written in (35) and shown in Fig. 1, what occurs on the left-hand side of the gap equation is the

space-dependent condensate from (21),

$$C_F(\mathbf{x})_{ij} = \sum_I \sum_{I'ij} (q_I^a) e^{2iq_I^a \cdot \mathbf{x}}; \tag{37}$$

whereas we now wish to turn the gap equation into a set of coupled equations for the constants  $(q_I^a)$ . Doing so requires simplification of the color-flavor structure of the right-hand side. Our ansatz for the color-flavor structure of the condensate, on the left-hand side, is antisymmetric in both color and flavor.

However, direct evaluation of the right-hand side yields terms that are symmetric in color and flavor, in addition to the desired terms that are antisymmetric in both. This circumstance is familiar from the analysis of the CFL phase [1, 5], whose color-flavor structure we are after all employing. In the presence of a color and flavor antisymmetric condensate, a symmetric condensate must also be generated because doing so does not change any symmetries. The same argument applies here also. In the CFL phase, the symmetric condensate is both quantitatively and parametrically suppressed relative to the antisymmetric condensate, which is understandable based on the basic fact that the QCD interaction is attractive in the antisymmetric channel and repulsive in the symmetric channel. We therefore expect that here too if we were to include color and flavor symmetric condensates in our ansatz and solve for them, they would prove to be suppressed relative to the antisymmetric condensates, and furthermore expect that, as in the CFL phase, their inclusion would have negligible impact on the value of the dominant

antisymmetric condensate. Hence, we drop the color and flavor symmetric terms occurring on the right-hand side of the gap equation. Upon so doing, the right-hand side of the gap equation, which we denote  $R_{ij}$ , has the structure

$$R_{ij}(x) = \sum_I R_I(x) \Gamma_{Iij} \quad (38)$$

Because  $\Gamma_{Iij}$  are linearly independent tensors for each value of  $I$ , in order for the gap equation to be satisfied for all values of  $x, i$  and  $j$  we must have

$$\sum_I (q_I^a) e^{2iq_I^a x} = R_I(x) \quad (39)$$

for all three values of  $I$ . This is a set of  $\sum_I P_I$  coupled equations for the undetermined constants  $(q_I^a)$ . (Recall that  $P_I$  is the number of vectors in the set  $fq_I g$ .) After transforming to momentum space, these gap equations can be written as follows:



$$\begin{aligned}
(q_I^a) = & \frac{2}{2} \sum_{q_I^b} (q_I^b)_{jk} (q_I^b; q_I^a)_{q_I^b q_I^a} \\
& + \sum_{q_I^b q_I^c q_I^d} (q_I^b) (q_I^c) (q_I^d) J_{jkjk} (q_I^b; q_I^c; q_I^d; q_I^a)_{q_I^b q_I^c + q_I^d q_I^a} \\
& + \frac{1}{2} \sum_{q_J^b q_J^c q_I^d} (q_J^b) (q_J^c) (q_I^d) J_{kIkJ} (q_J^b; q_J^c; q_I^d; q_I^a)_{q_J^b q_J^c + q_I^d q_I^a} \\
& + \sum_{q_I^b q_I^c q_I^d q_I^e} (q_I^b) (q_I^c) (q_I^d) (q_I^e) (q_I^f) K_{jkjkjk} (q_I^b; q_I^c; q_I^d; q_I^e; q_I^f; q_I^a)_{q_I^b q_I^c + q_I^d q_I^e + q_I^f q_I^a} \\
& + \sum_{q_J^b q_J^c q_I^d q_I^e q_I^f} (q_J^b) (q_J^c) (q_I^d) (q_I^e) (q_I^f) K_{kIkJkI} (q_J^b; q_J^c; q_I^d; q_I^e; q_I^f; q_I^a)_{q_J^b q_J^c + q_I^d q_I^e + q_I^f q_I^a} \\
& + \frac{1}{2} \sum_{q_J^b q_J^c q_J^d q_I^e q_I^f} (q_J^b) (q_J^c) (q_J^d) (q_I^e) (q_I^f) K_{kIkIkJ} (q_J^b; q_J^c; q_J^d; q_I^e; q_I^f; q_I^a)_{q_J^b q_J^c + q_J^d q_I^e + q_I^f q_I^a} \\
& + \frac{1}{2} \sum_{J,K} \sum_{q_I^b q_J^c q_K^d q_K^e q_J^f} (q_I^b) (q_J^c) (q_K^d) (q_K^e) (q_J^f) K_{JKIJIK} (q_I^b; q_J^c; q_K^d; q_K^e; q_J^f; q_I^a)_{q_I^b q_J^c + q_K^d q_K^e + q_J^f q_I^a} \\
& + \frac{1}{4} \sum_{J,K} \sum_{q_J^b q_J^c q_K^d q_K^e q_K^f} (q_J^b) (q_J^c) (q_I^d) (q_K^e) (q_K^f) K_{KIKJJI} (q_J^b; q_J^c; q_I^d; q_K^e; q_K^f; q_I^a)_{q_J^b q_J^c + q_I^d q_K^e + q_K^f q_I^a} \\
& + \frac{1}{4} \sum_{J,K} \sum_{q_J^b q_K^c q_K^d q_K^e q_K^f} (q_J^b) (q_K^c) (q_I^d) (q_K^e) (q_K^f) K_{KIKJIK} (q_J^b; q_K^c; q_I^d; q_K^e; q_K^f; q_I^a)_{q_J^b q_K^c + q_I^d q_K^e + q_K^f q_I^a} ;
\end{aligned}$$

#

(40)

where we have introduced a lot of notation that we now define and explain. First, recall from (15) that  $q_I^b$  means a sum over all the  $q_I^b$ 's in the set  $fq_Ig$ . The  $\delta$ 's are therefore Kronecker  $\delta$ 's, indicating that only those  $q$ -vectors that can be arranged to form a certain closed two-, four- or six-sided figure in momentum space are to be included in the sum. The sums over  $J$  are always understood to be sums over  $J \notin I$ , and the sums over  $K$  are always understood to be sums over  $K \notin J$  and  $K \notin I$ . The remaining subscripts in some terms which are not

summed, denoted  $j$  or  $k$ , must always be chosen not equal to each other, not equal to  $I$ , and not equal to  $J$  if  $J$  occurs. (This appears to leave an ambiguity related to the exchange of  $j$  and  $k$  in terms where both occur, but we shall see that the functions  $J$  and  $K$  each have a cyclic symmetry that ensures that the two apparent choices of  $j$  and  $k$  are equivalent.) The functions  $J$ ,  $J$  and  $K$  are proportional to the various loop integrals that appear in the evaluation of the Feynman diagrams in the gap equation of Fig. 1. They are given by

$$\begin{aligned}
i_{ij}(k_1; k_2) &= \frac{i^{-2}}{2} \int \frac{d^4 p}{(2\pi)^4} \frac{1}{(p^2 - i)(p + 2k_1 + i)^2} \\
J_{i,j;k,l}(k_1; k_2; k_3; k_4) &= \frac{i^{-2}}{2} \int \frac{d^4 p}{(2\pi)^4} \frac{1}{(p^2 - i)(p + 2k_1 + i)(p + 2k_1 - 2k_2 - i)} \\
K_{i,j;k,l,m,n}(k_1; k_2; k_3; k_4; k_5; k_6) &= \frac{i^{-2}}{2} \int \frac{d^4 p}{(2\pi)^4} \frac{1}{(p^2 - i)(p + 2k_1 + i)(p + 2k_1 - 2k_2 + 2k_3 + i)(p + 2k_1 - 2k_2 + 2k_3 - 2k_4 - i)} \\
&\quad \frac{1}{(p + 2k_1 - 2k_2 + 2k_3 + i)(p + 2k_1 - 2k_2 + 2k_3 - 2k_4 - i)} ; \\
&\quad \frac{1}{(p + 2k_1 - 2k_2 + 2k_3 - 2k_4 + 2k_5 + i)} ;
\end{aligned} \tag{41}$$

where  $i = 0$  and  $k = (0; k)$ . The subscripts  $i, j$  etc. on the functions  $i, J$  and  $K$  are flavor indices that give the flavor of the quark lines in the propagators going around the loops in Fig. 1. In each term in (40) the choice of flavor indices in  $i, J$  or  $K$  is determined by the requirement that a given  $(q_I^a)$  must connect two propagators for quarks with flavors different from each other and  $I$ . For example,  $i_3$  always connects a  $u$  and a  $d$  quark. The easiest way to see how this provides the explanation for the (perhaps initially peculiar looking) prescriptions for the  $J$  and  $K$  functions in each term in the gap equations (40) is to examine Fig. 2 below, which depicts examples of the contributions

of  $i, J$  and  $K$  to the free energy which we shall discuss next.

The gap equations that we have derived must be equivalent to the set of equations  $\partial \mathcal{E} / \partial (q_I^a) = 0$ , because solutions to the gap equation are stationary points of the free energy. This means that integrating the gap equations determines up to an overall multiplicative constant, which we can fix by requiring that we reproduce known results for the single-plane wave condensates, and up to an additive constant which we fix by the requirement that  $\mathcal{E}_{\text{crystalline}} = \mathcal{E}_{\text{unpaired}}$  when all  $(q_I^a)$  are set to zero. We find

$$\begin{aligned}
(f(q_I^a)g) &= \frac{2^{-2} X}{2} \sum_I (q_I^b)(q_I^a)_{jk} (q_I^a; q_I^b) + \frac{2}{2^{-2}} q_I^b q_I^a \\
&+ \frac{1}{2} \sum_{q_I^b q_I^c q_I^d q_I^a} (q_I^b)(q_I^c)(q_I^d)(q_I^a) J_{jkjk} (q_I^b; q_I^c; q_I^d; q_I^a) q_I^b q_I^c + q_I^d q_I^a \\
&+ \frac{1}{2} \sum_{J > I} \sum_{q_J^b q_J^c q_I^d q_I^a} (q_J^b)(q_J^c)(q_I^d)(q_I^a) J_{kIkJ} (q_J^b; q_J^c; q_I^d; q_I^a) q_J^b q_J^c + q_I^d q_I^a \\
&+ \frac{1}{3} \sum_{q_I^b q_I^c q_I^d q_I^e q_I^f q_I^a} (q_I^b)(q_I^c)(q_I^d)(q_I^e)(q_I^f)(q_I^a) K_{jkjkjk} (q_I^b; q_I^c; q_I^d; q_I^e; q_I^f; q_I^a) q_I^b q_I^c + q_I^d q_I^e + q_I^f q_I^a \\
&+ \frac{1}{2} \sum_{J \notin I} \sum_{q_J^b q_J^c q_I^d q_I^e q_I^f q_I^a} (q_J^b)(q_J^c)(q_I^d)(q_I^e)(q_I^f)(q_I^a) \\
&\quad K_{kIkJkJ} (q_J^b; q_J^c; q_I^d; q_I^e; q_I^f; q_I^a) q_J^b q_J^c + q_I^d q_I^e + q_I^f q_I^a \\
&+ \frac{1}{4} \sum_{J \notin K \notin I \notin J} \sum_{q_I^b q_I^c q_K^d q_K^e q_J^f q_I^a} (q_I^b)(q_I^c)(q_K^d)(q_K^e)(q_J^f)(q_I^a) \\
&\quad K_{JKIJK} (q_I^b; q_J^c; q_K^d; q_K^e; q_J^f; q_I^a) q_I^b q_J^c + q_K^d q_K^e + q_J^f q_I^a \\
&+ \frac{1}{12} \sum_{J \notin K \notin I \notin J} \sum_{q_J^b q_K^c q_I^d q_J^e q_K^f q_I^a} (q_J^b)(q_K^c)(q_I^d)(q_J^e)(q_K^f)(q_I^a) \\
&\quad K_{KIJKIJ} (q_J^b; q_K^c; q_I^d; q_J^e; q_K^f; q_I^a) q_J^b q_K^c + q_I^d q_J^e + q_K^f q_I^a : \\
\end{aligned} \tag{42}$$

As in (40), in each term the flavor indices  $j$  and  $k$  (or just  $k$ ) that are not summed over are understood to differ from each other and from the summed indices  $I$  (or  $I$  and  $J$ ).

As we discussed in Section III, we shall only consider crystal structures in which each of the three sets  $f_{q_I} g$  are regular, in the sense that all the  $q_I^a$  in one set  $f_{q_I} g$  are equivalent. This means that  $(q_I^a) = 1$ , which simplifies the free energy (42) to the form (29) which we derived on general grounds in Section III and which we reproduce here

$$\begin{aligned}
(\phi_1; \phi_2; \phi_3) &= \frac{2^{-2} X}{2} \sum_I P_I \phi_I + \frac{1}{2} \sum_I \phi_I (\phi_I)^2 + \sum_{I > J} \phi_I \phi_J \phi_I \phi_J \phi_I \phi_J \\
&+ \frac{1}{3} \sum_{I \notin J} \phi_I (\phi_I)^3 + \sum_{I \notin J} \phi_I \phi_J \phi_I \phi_J \phi_I \phi_J \phi_I \phi_J + \phi_{123} \phi_1 \phi_1 \phi_2 \phi_2 \phi_3 \phi_3^A \\
\end{aligned} \tag{43}$$

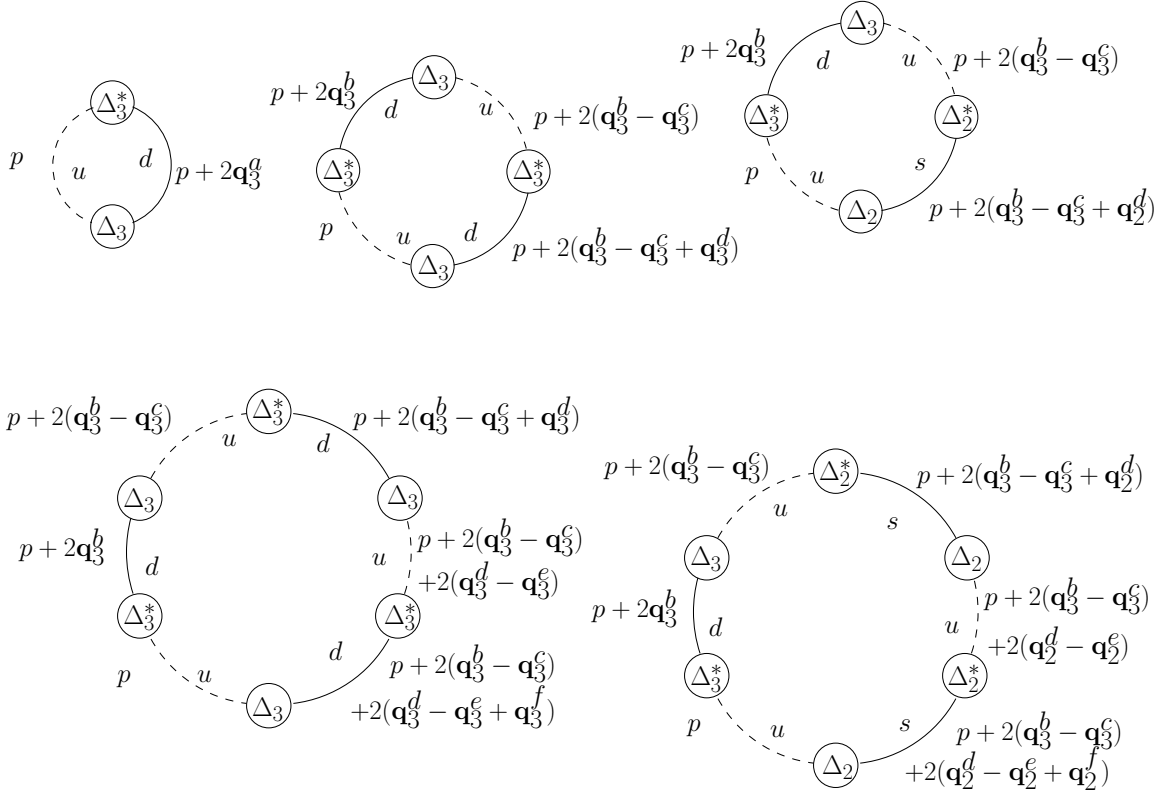


FIG. 2: Examples of contributions to the free energy. The five diagrams depict a  $J_{ud}$  contribution to  $\chi_3(\chi_3 - \chi_3)^2$ , a  $J_{udud}$  contribution to  $\chi_3(\chi_3 - \chi_3)^2$ , a  $J_{udus}$  contribution to  $\chi_3(\chi_3 - \chi_3)^2$ , a  $K_{ududud}$  contribution to  $\chi_3(\chi_3 - \chi_3)^2$  and a  $K_{udusus}$  contribution to  $\chi_3(\chi_3 - \chi_3)^2$ .

for continuity. Now, however, we have obtained explicit expressions for all of the coefficients:

$$\begin{aligned}
 I &= \sum_{jk} (q_I^a; q_I^a) + \frac{2}{2-2} \\
 I &= \sum_{q_I^b q_I^c q_I^d q_I^a} J_{jkjk} (q_I^b; q_I^c; q_I^d; q_I^a) q_I^b q_I^c + q_I^d q_I^a \\
 JI &= \sum_{q_J^b q_J^c q_I^d q_I^a} J_{kIkJ} (q_J^b; q_J^c; q_I^d; q_I^a) q_J^b q_J^c + q_I^d q_I^a \\
 I &= \sum_{q_I^b q_I^c q_I^d q_I^e q_I^f q_I^a} K_{jkjkjk} (q_I^b; q_I^c; q_I^d; q_I^e; q_I^f; q_I^a) q_I^b q_I^c + q_I^d q_I^e + q_I^f q_I^a \\
 JII &= \frac{3}{2} \sum_{q_J^b q_J^c q_I^d q_I^e q_I^f q_I^a} K_{kIkJkJ} (q_J^b; q_J^c; q_I^d; q_I^e; q_I^f; q_I^a) q_J^b q_J^c + q_I^d q_I^e + q_I^f q_I^a \\
 123 &= \frac{3}{4} \sum_{I \in J \in K \in I} \sum_{q_J^b q_J^c q_I^d q_I^e q_I^f q_I^a} K_{JKIJIK} (q_J^b; q_J^c; q_I^d; q_I^e; q_I^f; q_I^a) q_J^b q_J^c + q_I^d q_I^e + q_I^f q_I^a \\
 &\quad + \frac{1}{4} \sum_{I \in J \in K \in I} \sum_{q_J^b q_J^c q_I^d q_I^e q_I^f q_I^a} K_{KIJKIJ} (q_J^b; q_J^c; q_I^d; q_I^e; q_I^f; q_I^a) q_J^b q_J^c + q_I^d q_I^e + q_I^f q_I^a :
 \end{aligned} \tag{44}$$

Here again, the unsummed indices  $j$  and  $k$  are chosen as described previously. Since the free energy (43) is invariant under phase rotations of the  $\mathbf{r}_I$  we can henceforth take all the  $\mathbf{r}_I$  real and positive. In Fig. 2, we give examples of contributions to the free energy. These examples should make clear the choice of flavor subscripts on the  $J$ 's and  $K$ 's in (44) and consequently in (40). They also illustrate the origin of the Kronecker  $\delta$ 's in so many of the expressions in this section: each insertion of a  $(\mathbf{q}_I^a)$  (or  $(\mathbf{q}_I^{\bar{a}})$ ) adds (or subtracts) momentum  $2\mathbf{q}_I^a$  to (from) the loop, meaning that the Kronecker  $\delta$ 's arise due to momentum conservation. The diagrams also illustrate that  $J$ ,  $J$  and  $K$  are invariant under simultaneous cyclic permutation of their flavor indices and momentum arguments, as this corresponds simply to rotating the corresponding diagrams.

We have succeeded in deriving expressions for the Ginzburg-Landau coefficients in our model; we shall turn to evaluating them in the next section. Recall, however, that upon setting  $\mathbf{r}_I = 0$  and keeping in mind that we can obtain results for  $\mathbf{r}_I$ ,  $\mathbf{r}_I$  and  $\mathbf{r}_I$  from the two-flavor analyses in Ref. [35], all that we need to do is evaluate  $\mathcal{J}_{32}$ ,  $\mathcal{J}_{233}$  and  $\mathcal{J}_{322}$  for the crystal structures we wish to investigate. We shall largely focus on crystal structures for which  $\mathbf{f}\hat{\mathbf{q}}_2\mathbf{g}$  and  $\mathbf{f}\hat{\mathbf{q}}_3\mathbf{g}$  are "exchange symmetric", meaning that there is a sequence of rigid rotations and reflections which when applied to all the vectors in  $\mathbf{f}\hat{\mathbf{q}}_2\mathbf{g}$  and  $\mathbf{f}\hat{\mathbf{q}}_3\mathbf{g}$  together has the effect of exchanging  $\mathbf{f}\hat{\mathbf{q}}_2\mathbf{g}$  and  $\mathbf{f}\hat{\mathbf{q}}_3\mathbf{g}$ . If we choose an exchange symmetric crystal structure, upon making the approximation that  $\mathbf{r}_2 = \mathbf{r}_3$  and restricting our attention to solutions with  $\mathbf{r}_2 = \mathbf{r}_3$  we have the further simplification that  $\mathcal{J}_{322} = \mathcal{J}_{233}$ . Once we learn how to evaluate the loop integrals  $J$  and  $K$  in the next Section, we will then in Section V I evaluate  $\mathcal{J}_{32}$  and  $\mathcal{J}_{322}$  for various crystal structures, enabling us to evaluate the magnitudes of their gaps and condensation energies.

## V. CALCULATING GINZBURG-LANDAU COEFFICIENTS

Calculating the Ginzburg-Landau coefficients (44) that specify  $(\mathbf{r}_1; \mathbf{r}_2; \mathbf{r}_3)$  for a given crystal structure involves first evaluating the loop integrals  $J$ ,  $J$  and  $K$ , defined in (41), and then summing those that contribute to a given Ginzburg-Landau coefficient. For example, we see from (44) that the Ginzburg-Landau coefficient  $\mathcal{J}_{32}$  is given by sum-

ming  $J_{\text{udus}}(\mathbf{q}_3^b; \mathbf{q}_3^c; \mathbf{q}_2^d; \mathbf{q}_2^{\bar{d}})$  over all those vectors  $\mathbf{q}_3^b$  and  $\mathbf{q}_3^c$  in the set  $\mathbf{f}\hat{\mathbf{q}}_3\mathbf{g}$  and all those vectors  $\mathbf{q}_2^d$  and  $\mathbf{q}_2^{\bar{d}}$  in the set  $\mathbf{f}\hat{\mathbf{q}}_2\mathbf{g}$  which satisfy  $\mathbf{q}_3^b + \mathbf{q}_3^c + \mathbf{q}_2^d + \mathbf{q}_2^{\bar{d}} = 0$ , forming a closed four-sided figure in momentum space. Understanding how to evaluate the loop integrals  $J$ ,  $J$  and  $K$  requires some explanation, which is our goal in this section. Performing the sum required to evaluate a given Ginzburg-Landau coefficient is then just bookkeeping, albeit nontrivial bookkeeping for complicated crystal structures.

We are working in a weak-coupling limit in which  $\mathbf{r}_I \ll \mathbf{q} = \mathbf{r}_I$ , and  $\mathbf{r}_{2SC}$  are all much smaller than  $\mathbf{r}_I$ . This means that we can choose our cutoff such that  $\mathbf{r}_I \gg \mathbf{r}_{2SC}$ . Because  $\mathbf{r}_I$ , the integration measure in the expressions (41) for  $J$ ,  $J$  and  $K$  simplifies as follows:

$$\frac{d^4p}{(2\pi)^4} \rightarrow \frac{d^4p}{(2\pi)^4} \frac{ds}{2} \frac{d\phi}{4}; \quad (45)$$

where  $s = |\mathbf{p}|$ . We now see by power counting that  $\mathcal{J}_{32}$  is log-divergent as we take  $\mathbf{r}_I \gg \mathbf{r}_{2SC}$  whereas both  $J$  and  $K$  are  $\mathbf{r}_I$ -independent in the large limit. Thus, in evaluating  $J$  and  $K$ , we can safely take  $\mathbf{r}_I \gg \mathbf{r}_{2SC}$  whereas we must keep  $\mathbf{r}_I$  in the problem for a little longer in analyzing  $\mathcal{J}_{32}$ . Explicit evaluation of  $\mathcal{J}_{32}$  yields

$$\mathcal{J}_{32}(\mathbf{q}_3; \mathbf{q}_3) = 1 + \frac{3}{2q_3} \log \frac{q_3 + \frac{3}{2}}{q_3 - \frac{3}{2}} - \frac{1}{2} \log \frac{2}{q_3^2 - \frac{9}{4}}; \quad (46)$$

We can now use

$$\mathcal{J}_{2SC} = 2e^{-\frac{2}{\mathbf{r}_I^2}} \quad (47)$$

and the relation between  $\mathbf{r}_3$  and  $\mathbf{r}_{\text{ud}}$  given in (44) to evaluate  $\mathcal{J}_{32}$ , obtaining the result (30). Notice that  $\mathbf{r}_I$  depends on  $\mathbf{r}_I$  and only through  $\mathbf{r}_{2SC}$ , and depends only on the ratios  $q_I = \mathbf{r}_I / \mathbf{r}_{2SC}$  and  $\mathbf{r}_I = \mathbf{r}_{2SC}$ . As discussed in Section III,  $\mathbf{r}_I$  is negative for  $\mathbf{r}_I = \mathbf{r}_{2SC} < 0.754$ , and for a given value of this ratio for which  $\mathbf{r}_I < 0$ ,  $\mathbf{r}_I$  is most negative for  $q_I = \mathbf{r}_{2SC} = \mathbf{r}_I = \mathbf{r}_{2SC}$  with  $\mathbf{r}_I = 1.1997$ . We therefore set  $q_I = \mathbf{r}_I$  henceforth and upon so doing



obtain

$$\begin{aligned} (\gamma_I) &= 1 + \frac{1}{2} \log \frac{1 + \frac{1}{2}}{1} \\ &= \frac{1}{2} \log \frac{1 + \frac{1}{2}}{1} \\ &= \frac{1}{2} \log \frac{1 + \frac{1}{2}}{1} ; \end{aligned} \quad (48)$$

where in the last line we have used the definition of  $\gamma_I$  derived from (30).

The evaluation of  $\gamma_I$  and  $\gamma_{2SC}$  is described in Ref. [35]. From the integration measure (45) and the definitions of  $J$  and  $K$  (41) we see that  $\gamma_I$  and  $\gamma_{2SC}$  have dimension -2 and -4, respectively. Since they are independent of  $\mu$  as long as  $\mu \gg \Lambda_{2SC}$ , and since  $\Lambda_{2SC}$  now here appears in their definition, there is no need to introduce  $\Lambda_{2SC}$ . This means that the only dimensionful quantity on which they can depend is  $\Lambda_I$  (since  $q_I = \Lambda_I$  and since the propagators are independent of  $\mu$  in the weak-coupling limit) and so we can write

$$\gamma_I = \frac{1}{2} \Lambda_I^{-2} \text{ and } \gamma_{2SC} = \frac{1}{4} \Lambda_I^{-4} ; \quad (49)$$

where  $\gamma_I$  and  $\gamma_{2SC}$  are dimensionless quantities that depend only on the shape of the polyhedron described by the set of vectors  $f_{q_I} g$ . The evaluation of the  $J$  and  $K$  loop integrals occurring in (48) and (49) is described in Ref. [35], and results for many two-avor crystal structures  $f_{q_3} g$  are tabulated there. The evaluation is similar to but simpler than the evaluation of  $\gamma_{32}$  and  $\gamma_{322}$ , to which we now turn.

$\gamma_{32}$  is the sum of  $J_{\text{udus}}(q_3^b; q_3^c; q_2^d; q_2^a)$ , where the momentum vectors satisfy

$$q_3^b = q_3^c + q_2^d = q_2^a = 0 ; \quad (50)$$

We now utilize the fact that  $\mathbf{f}_{q_3^b} = \mathbf{f}_{q_3^c} = \mathbf{f}_{q_2^d} = \mathbf{f}_{q_2^a}$  and  $\mathbf{f}_{q_2^d} = \mathbf{f}_{q_2^a} = \mathbf{f}_{q_3^b} = \mathbf{f}_{q_3^c}$  where  $\mathbf{f}_{q_3}$  and  $\mathbf{f}_{q_2}$  are similar in magnitude, but not precisely equal. (Recall from Section IIA that both are given by  $M_s^{-2} = (8/\Lambda_s^2)$  to this order, but that they differ at order  $M_s^{-4} = 3/\Lambda_s^4$ .) Because  $\mathbf{f}_{q_2} \notin \mathbf{f}_{q_3}$ , the condition (50) can only be satisfied if  $q_3^b = q_3^c$ , and  $q_2^d = q_2^a$ . We must therefore evaluate

$$J_{\text{udus}}(q_3^b; q_3^b; q_2^a; q_2^a) = \frac{1}{2} \int \frac{d^4 p}{(2\pi)^4} \frac{1}{(p^0 - \bar{u})(p^0 + 2q_3^b + \bar{u})(p^0 - \bar{u})(p^0 + 2q_2^a + \bar{s})} \quad (51)$$

We now expand the propagators in the weak-coupling limit, in which  $p^0, s, \bar{u}, \bar{s}$  ( $\sim \Lambda_u$ ) and  $(\bar{u} - s)$  are all small compared to  $\Lambda_u$ , as follows:

$$\begin{aligned} \frac{1}{p^0 + 2q_3^b + \bar{u}} &= \frac{(p^0 + \bar{u})^0 (p^0 + 2q_3^b)}{(p^0 + \bar{u})(p^0 + 2q_3^b)(p^0 + \bar{u} + p^0 + 2q_3^b)} \\ &= \frac{1}{(p^0 + \bar{u})^2} \frac{p^0}{p^0 + 2q_3^b} : \end{aligned} \quad (52)$$

Similarly,

$$\frac{1}{p^0 + 2q_2^a + \bar{s}} = \frac{1}{2} \frac{p^0 + \bar{s}}{p^0 + s + (\bar{u} - s) + 2q_2^a} : \quad (53)$$

Eq. (51) then simplifies to

$$J_{\text{udus}}(q_3^b; q_3^b; q_2^a; q_2^a) = \frac{1}{4} \int \frac{d^4 p}{(2\pi)^4} \frac{1}{(p^0 + s)^2 (p^0 - s - \bar{p} - 2q_3^b + 2q_2^a) (p^0 - s - \bar{p} - 2q_2^a + 2q_2^a)} \quad (54)$$

where we have used  $\bar{u} = \frac{1}{2}(\bar{u} - s)$  and  $\bar{s} = \frac{1}{2}(\bar{u} - s)$ .

To integrate (54), we Wick rotate  $p^0$  to  $ip^4$  and then do the  $s$  integral by contour integration. This gives two contributions with different sign factors,  $\text{sign}(p^4)$  and  $\text{sign}(-p^4)$ , which are complex conjugates of each other. Combining the two, the integration over  $p^4$  is of form  $2 < e^{R+1} dp^4$  (:) where we

have started the  $p^4$  integration from the infinitesimal positive number instead of zero, thus defining the principal value of the integral. The integration over  $p^4$  can now be carried out safely to obtain

$$\begin{aligned} J_{\text{udus}}(q_3^b; q_3^b; q_2^a; q_2^a) &= \frac{1}{4} \int_{-\infty}^{\infty} \frac{dp^4}{4} < e^{\frac{1}{4} \int_{-\infty}^{\infty} \frac{dp^4}{4}} \frac{1}{(i p^4 + 3)(i p^4 + 2)} \\ &= \frac{1}{4} \int_{-\infty}^{\infty} \frac{dp^4}{4} < e^{\frac{1}{4} \int_{-\infty}^{\infty} \frac{dp^4}{4}} \frac{1}{(i p^4 + 1)(i p^4 + 1)} ; \end{aligned} \quad (55)$$

where  $\frac{1}{4} \int_{-\infty}^{\infty} \frac{dp^4}{4} = \frac{1}{2} \int_{-\infty}^{\infty} \frac{dp^4}{4}$ . From rotational symmetry it follows that the value of (55) depends only on the angle between the momentum vectors  $q_3^b$  and  $q_2^a$ , which we denote by  $\theta$ . We therefore define the dimensionless quantities

$$J_{32}(\theta) = \frac{1}{4} \int_{-\infty}^{\infty} \frac{dp^4}{4} J_{\text{udus}}(q_3^b; q_3^b; q_2^a; q_2^a) \quad (56)$$

and, correspondingly,

$$J_{32} = \frac{1}{4} \int_{-\infty}^{\infty} \frac{dp^4}{4} J_{32}(\theta) \quad (57)$$

$J_{32}$  can be evaluated analytically by using Feynman parameters to simplify the integrand in (55). The result is

$$J_{32}(\theta) = \frac{1}{4} \int_{-\infty}^{\infty} \frac{dp^4}{4} \frac{1}{\cos(\theta/2)} \arctan \left( \frac{\sin(\theta/2)}{\cos(\theta/2)} \right) \quad (58)$$

This completes the evaluation of the loop integral  $J$  needed to calculate  $J_{32}$  for any crystal structure. We summarize the calculation by noting that for a given crystal structure,  $J_{32}$  depends only on the shape of the polyhedron defined by  $f_{q_2g}$  and  $f_{q_3g}$  and on their relative orientation, depends on the Fermi surface splittings  $\epsilon_3$  and  $\epsilon_2$ , and is obtained using (57) with

$$J_{32} = \sum_{q_3^b, q_2^a} J_{32}(\theta_{q_3^b, q_2^a}) \quad (59)$$

where  $J_{32}(\theta)$  is given by (58).

We turn now to the evaluation of  $J_{322}$ . From (44),

$$J_{322} = \frac{3}{2} \sum_{\substack{q_3^b, q_3^c; \\ q_2^d, q_2^e, q_2^f, q_2^a}} K_{\text{udus}}(q_3^b; q_3^c; q_2^d; q_2^e; q_2^f; q_2^a) \quad (60)$$

and we again use the fact that the  $q_3$ 's and  $q_2$ 's do not have precisely the same length to conclude that the momentum vectors must satisfy both

$$q_3^b = q_3^c \quad (61)$$

and

$$q_2^d = q_2^e + q_2^f - q_2^a = 0 \quad (62)$$

In the following expressions, it is always understood that (62) is satisfied although we will not complicate

equations by eliminating one of the  $q_2$ 's in favor of the other three. We can see without calculation that, unlike  $J, K$  will not reduce to depending only on a single angle between two momentum vectors. It will depend on the shape made by the four  $q_2$  vectors satisfying (62), which can in fact be specified by two

angles, as well as on the angles that specify the direction of  $q_3^b$  relative to the shape made by the four  $q_2$ 's.

The expression for  $K$  is given in (41) and can also be read off from the bottom right Feynman diagram in Fig. 2. It is given by

$$K_{\text{udusus}}(q_3^b; q_3^b; q_2^d; q_2^e; q_2^f; q_2^a) = \frac{i^2}{2} \int \frac{d^4 p}{(2\pi)^4} \frac{1}{(p^0 - \bar{u})(p + 2q_3^b - \bar{u})(p - \bar{u})} \frac{1}{(p + 2q_2^d + \bar{s})(p + 2(q_2^d - q_2^e) - \bar{u})(p + 2(q_2^d - q_2^e + q_2^f) + \bar{s})} : \quad (63)$$

After simplifying the propagators using (52), we can rewrite equation (63) as

$$K_{\text{udusus}}(q_3^b; q_3^b; q_2^d; q_2^e; q_2^f; q_2^a) = \int \frac{d\bar{p}}{4} \int_1^{Z+1} \frac{d\bar{p}^0}{2i} \int_1^{Z+1} ds \frac{1}{(p^0 + s)^2 (p^0 + s + \bar{p} - 2(q_1^d - q_2^e))} \frac{1}{(p^0 - s - \bar{p} - 2q_1 + 2q_3)(p^0 - s - \bar{p} - 2q_1 - 2q_2)(p^0 - s - \bar{p} - 2(q_1 - q_2 + q_2^f) - 2q_2)} : \quad (64)$$

Unlike in the evaluation of  $J_{\text{udus}}$ , we are not able to do the  $s$  and  $p^0$  integrals analytically without introducing Feynman parameters to simplify the integrand at this stage, before doing any of the integrals. We introduce one set of Feynman parameters,  $x_1; x_2$ , to collect denominators of the form  $p^0 + s + \dots$  and another set,  $y_1; y_2; y_3$ , to collect the denominators of form  $p^0 - s + \dots$ . This reduces the integral to

$$K_{\text{udusus}}(q_3^b; q_3^b; q_2^d; q_2^e; q_2^f; q_2^a) = \int_0^1 \int_0^1 dx_n \int_0^1 \int_0^1 dy_m \int_0^1 \int_0^1 dy_m \frac{1}{(p^0 + s + 2x_2 \bar{p} - 2(q_1^d - q_2^e))^3} \frac{1}{(p^0 - s - \bar{p} - [q_3^b + y_2 q_2^d + y_3 (q_2^d - q_2^e + q_2^f)] + y_1 2q_3 - y_2 2q_2 - y_3 2q_2)} : \quad (65)$$

We now perform the  $p^0$  and  $s$  integrations in (65), following steps analogous to the integration arising in the expression for  $J_{\text{udus}}$ . i.e. Wick rotate  $p^0$  to  $ip^4$ , do the  $s$  integral by contour integration, add the two complex conjugate contributions thus obtained to write the integration over  $p^4$  as  $2 < e^{i\pi} dp^4$  (:) and then perform the integration over  $p^4$ . This gives us

$$K_{\text{udusus}}(q_3^b; q_3^b; q_2^d; q_2^e; q_2^f; q_2^a) = \frac{3}{8} < e^{i\pi} \int_0^1 \int_0^1 dx_n \int_0^1 \int_0^1 dy_m \int_0^1 \int_0^1 dy_m \frac{1}{(i + \bar{p} - [q_2^d - q_2^e] - [q_3^b + y_2 q_2^d + y_3 (q_2^d - q_2^e + q_2^f)] + y_1 2q_3 - y_2 2q_2 - y_3 2q_2)} : \quad (66)$$

Finally, we do the  $d\mathbf{p}$  integral and obtain

$$K_{\text{udusus}}(q_3^b; q_3^b; q_2^d; q_2^e; q_2^f; q_2^a) = \frac{1}{8} \int_0^1 \int_{\mathbf{x}_n}^{Y^2} \int_{\mathbf{x}_n}^{X^2} \int_0^1 \int_{\mathbf{y}_m}^{Y^3} \int_{\mathbf{y}_m}^{X^3} (1 - \mathbf{x}_2) \frac{[\mathbf{x}_2(q_2^d - q_2^e) - (\mathbf{y}_1 q_3^b + \mathbf{y}_2 q_2^d + \mathbf{y}_3(q_2^d - q_2^e + q_2^f))]^2 + 3[\mathbf{y}_1^2 - \mathbf{y}_2^2 - \mathbf{y}_3^2]^2}{[\mathbf{x}_2(q_2^d - q_2^e) - (\mathbf{y}_1 q_3^b + \mathbf{y}_2 q_2^d + \mathbf{y}_3(q_2^d - q_2^e + q_2^f))]^2 - [\mathbf{y}_1^2 - \mathbf{y}_2^2 - \mathbf{y}_3^2 + i]} : \quad (67)$$

Noting that we can replace  $q_2$  by  $\hat{q}_2$  and  $q_3$  by  $\hat{q}_3$ , we conclude that, as expected,  $K_{\text{udusus}}$  depends only upon the shape of the polyhedra defined by  $\mathbf{f}q_2\mathbf{g}$  and  $\mathbf{f}q_3\mathbf{g}$  and on the Fermi surface splittings  $\beta_3$  and  $\beta_2$ . We cannot simplify (67) further for general  $\beta_2, \beta_3$ . However, if we now set  $\beta_2 = \beta_3 = 0$ , which is corrected only at order  $M_s^{-4} = \beta^3$ , we can then factor out the dependence on the Fermi surface splitting, since the only dimensional quantity in the integrand is then  $\beta$ . Denoting, for  $\beta_2 = \beta_3 = 0$ ,

$$K_{\text{udusus}}(q_3^b; q_3^b; q_2^d; q_2^e; q_2^f; q_2^a) = \frac{1}{4} K_{322}(q_3^b; q_3^b; q_2^d; q_2^e; q_2^f; q_2^a); \quad (68)$$

and using  $\mathbf{p}_1 = -\mathbf{p}_2$ , for all the momentum vectors, we find that  $K_{322}$  is given by

$$K_{322}(q_3^b; q_3^b; q_2^d; q_2^e; q_2^f; q_2^a) = \frac{1}{8} \int_0^1 \int_{\mathbf{x}_2}^{Y^2} \int_{\mathbf{x}_2}^{X^2} \int_0^1 \int_{\mathbf{y}_1}^{Y^3} \int_{\mathbf{y}_1}^{X^3} dy_2 < e^{-\frac{2[\mathbf{x}_2(\mathbf{x}_2; \mathbf{y}_1; \mathbf{y}_2)]^2 + 3(1 - 2\mathbf{y}_1)^2}{[2[\mathbf{x}_2(\mathbf{x}_2; \mathbf{y}_1; \mathbf{y}_2)]^2 - (1 - 2\mathbf{y}_1)^2 + i]}}; \quad (69)$$

where

$$a = \mathbf{x}_2 \cdot \hat{q}_2^d - \hat{q}_2^e - \mathbf{y}_1 \hat{q}_3^b + \mathbf{y}_2 \hat{q}_2^d + (1 - \mathbf{y}_1 - \mathbf{y}_2)(\hat{q}_2^d - \hat{q}_2^e + \hat{q}_2^f) : \quad (70)$$

For general arguments we were not able to do the integrals that remain in (69) analytically and therefore evaluated it numerically. Since  $K_{322}(q_3^b; q_3^b; q_2^d; q_2^e; q_2^f; q_2^a)$  is the limit of the function  $K_{322}(q_3^b; q_3^b; q_2^d; q_2^e; q_2^f; q_2^a; \beta)$  as  $\beta \rightarrow 0$ , we numerically evaluated the integral appearing in (69) at four values of  $\beta$  and extrapolated (using a cubic polynomial to fit the values) to  $\beta = 0$ . Finally

$$K_{322} = K_{322}^4 \quad (71)$$

is found by summing  $K_{322}$  evaluated with all possible choices of momentum vectors  $(q_3^b; q_3^b; q_2^d; q_2^e; q_2^f; q_2^a)$  satisfying (62) and multiplying this sum by 3=2.

## V I. R E S U L T S

### A . G e n e r a l i t i e s

We shall assume that  $\beta_1 = 0$  throughout this section. As described previously, this simplification is

motivated by the fact that  $\beta_1$  describes the pairing of d and s quarks, whose Fermi surfaces are twice as far apart from each other as either is from that of the u quarks. We shall focus most of our attention on exchange symmetric crystal structures, as defined at the end of Section IV, in which the polyhedra defined by  $\mathbf{f}q_2\mathbf{g}$  and  $\mathbf{f}q_3\mathbf{g}$  are related by a rigid rotation. In Section VI D we will discuss one example in which  $\mathbf{f}q_2\mathbf{g}$  and  $\mathbf{f}q_3\mathbf{g}$  are not exchange symmetric, and we have evaluated others. However, as none that we have investigated prove to be favorable, we shall make the notational simplifications that come with assuming that  $\mathbf{f}q_2\mathbf{g}$  and  $\mathbf{f}q_3\mathbf{g}$  are exchange symmetric, as this implies  $\beta_2 = \beta_3$ ,  $P_2 = \dim \mathbf{f}q_2\mathbf{g} = P_3 = \dim \mathbf{f}q_3\mathbf{g} = P$ ,  $\beta_2 = \beta_3$  and  $K_{322} = K_{233}$ . The final simplification we employ is to make the approximation that  $\beta_2 = \beta_3 = M_s^2 = (8)$ . As described in Section II A, this approximation is corrected by terms of order  $M_s^{-4} = \beta^3$ . Upon making all these simplifying assumptions and approximations, the free energy (43)

reduces to

$$\begin{aligned}
 (\rho_2; \rho_3) = & \frac{2}{2} \rho^2 P(\rho) \rho^2 + \frac{2}{3} \\
 & + \frac{1}{2} \frac{1}{\rho^2} (\rho^4 + \rho^4) + 32 \frac{2}{2} \frac{2}{3} \\
 & + \frac{1}{3} \frac{1}{\rho^4} (\rho^6 + \rho^6) + 322 (\frac{2}{2} \frac{4}{3} + \frac{4}{2} \frac{2}{3}) ; \quad \# \\
 \end{aligned} \quad (72)$$

where  $\rho$ ,  $\rho$ ,  $32$  and  $322$  are the dimensionless constants that we must calculate for each crystal structure as described in Section V, and where the dependence of  $\rho$  is given by Eq. (48).

In order to find the extrema of  $(\rho_2; \rho_3)$  in  $(\rho_2; \rho_3)$ -space, it is convenient to write  $(\rho_2; \rho_3)$  as  $2(\rho \cos \theta; \rho \sin \theta)$  in terms of which the free energy (72) is given by

$$\begin{aligned}
 (\rho; \theta) = & \frac{2}{2} 2P(\rho) \rho^2 + \frac{2}{2} \rho^4 + \frac{8}{3} \rho^6 \\
 & + \frac{4}{2} \frac{\rho}{\rho^2} (32 \rho^2) + \frac{2}{3} \frac{\rho}{\rho^4} (322 \rho^3) \sin^2 \theta : \quad \# \\
 \end{aligned} \quad (73)$$

Because  $\sin^2 \theta$  has extrema only at  $\theta = 0$  and  $\theta = \pi/2$ , we see that extrema of  $(\rho_2; \rho_3)$  either have  $\rho_2 = \rho_3 = \rho$ , or have one of  $\rho_2$  and  $\rho_3$  vanishing. The latter class of extrema are two-avor crystalline phases. We are interested in the solutions with  $\rho_2 = \rho_3 = \rho$ . The stability of these solutions relative to those with only one of the  $\rho$ 's nonzero appears to be controlled by the sign of the factor that multiplies  $\sin^2 \theta$  in (73). However, we shall show in Appendix A that the three-avor crystalline phases that we construct, with  $\rho_2 = \rho_3 = \rho$ , are electrically neutral whereas the two-avor solutions in which only one of the  $\rho$ 's is nonzero are not. Setting  $\rho_2 = \rho_3 = \rho$ , the free energy becomes

$$(\rho) = \frac{2}{2} 2P(\rho) \rho^2 + \frac{4}{2} \rho^4 + \frac{6}{3} \rho^6 ; \quad (74)$$

where we have defined

$$\begin{aligned}
 \rho_e &= 2 + 32 \\
 \rho_e &= 2 + 2 \cdot 322 : \quad (75)
 \end{aligned}$$

We have arrived at a familiar-looking sextic order Ginzburg-Landau free energy function, whose coefficients we will evaluate for specific crystal structures in VIB and VID. First, however, we review the physics described by this free energy depending on whether  $\rho_e$  and  $\rho_e$  are positive or negative.

If  $\rho_e$  and  $\rho_e$  are both positive, the free energy (74) describes a second order phase transition between the crystalline color superconducting phase and the normal phase at the  $\rho$  at which  $\rho$  changes sign. From (48), this critical point occurs where  $\rho = 0.754 \rho_{2SC}$ . In plotting our results, we will take the CFL gap to be  $\rho_0 = 25$  MeV, making  $\rho_{2SC} = 2^{1/3} \rho_0 = 31.5$  MeV. Recalling that  $\rho = M_s^2(8)$ , this puts the second order phase transition at

$$\begin{aligned}
 \frac{M_s^2}{\rho} &= 6.03 \rho_{2SC} = 7.60 \rho_0 = 190.0 \text{ MeV} : \\
 &= 0 \quad (76)
 \end{aligned}$$

(The authors of Refs. [39, 41] neglected to notice that it is  $\rho_{2SC}$ , rather than the CFL gap  $\rho_0$ , that occurs in Eqs. (30) and (48) and therefore controls the  $\rho$  at which  $\rho = 0$ . In analyzing the crystalline phase in isolation, this is immaterial since either  $\rho_0$  or  $\rho_{2SC}$  could be taken as the parameter defining the strength of the interaction between quarks. However, in Section VIE we shall compare the free energies of the CFL, gCFL and crystalline phases, and in making this comparison it is important to take into account that  $\rho_{2SC} = 2^{1/3} \rho_0$ .) For values of  $M_s^2 = \rho$  that are smaller than (76) (that is, lower densities),  $\rho < 0$  and the free energy is minimized by a nonzero  $\rho = \rho_{min}$  given by

$$\rho_{min} = \frac{\rho}{\frac{1}{2 \rho_e} \rho_e + \frac{2}{\rho_e} 8P(\rho) \rho_e} ; \quad (77)$$

and thus describes a crystalline color superconducting phase.

If  $\rho_e < 0$  and  $\rho_e > 0$ , then the free energy (74) describes a first order phase transition between unpaired and crystalline quark matter occurring at

$$\rho = \frac{3 \rho_e^2}{32 P(\rho_e)} : \quad (78)$$

At this positive value of  $\rho$ , the function  $\rho$  has a minimum at  $\rho = 0$  with  $\rho = 0$ , initially rises quadratically with increasing  $\rho$ , and is then turned back downward by the negative quartic term before



being turned back upwards again by the positive sextic term, yielding a second minimum at

$$= \frac{3j_e j}{4e}; \quad (79)$$

also with  $\epsilon = 0$ , which describes a crystalline color superconducting phase. For  $\epsilon < 0$ , the crystalline phase is favored over unpaired quark matter. Eq. (48) must be used to determine the value of  $\epsilon$ , and hence  $M_s^2 = \epsilon$ , at which  $\epsilon = 0$  and the first order phase transition occurs. If  $\epsilon > 0$ , the transition occurs at a value of  $M_s^2 = \epsilon$  that is greater than (76) by a factor  $(1 + \epsilon)$ . See Fig. 5 for an explicit example of plots of  $\epsilon$  versus  $\epsilon$  for various values of

for one of the crystal structures that we analyze in Section V D which turns out to have a first order phase transition.

A necessary condition for the Ginzburg-Landau approximation to be quantitatively reliable is that the sextic term in the free energy is small in magnitude compared to the quartic, meaning that

$2j_e = e j$ . If the transition between the unpaired and crystalline phases is second order, then this condition is satisfied close enough to the transition where  $\epsilon \neq 0$ . However, if  $\epsilon < 0$  and  $\epsilon > 0$ , making the transition first order, we see from (79) that at the first order transition itself  $\epsilon$  is large enough to make the quantitative application of the Ginzburg-Landau approximation marginal. This is a familiar result, coming about whenever a Ginzburg-Landau approximation predicts a first order phase transition because at the first order phase transition the quartic and sextic terms are balanced against each other. Even though it is quite a different problem, it is worth recalling the Ginzburg-Landau analysis of the crystallization of a solid from a liquid [50]. There too, a Ginzburg-Landau analysis predicts a first-order phase transition and thus predicts its own quantitative downfall. However, it remains important as a qualitative guide: it predicts a body-centered cubic crystal structure, and most elementary solids are body-centered cubic near their melting point. We shall find that our Ginzburg-Landau analysis predicts a first order phase transition; knowing that it is therefore at the edge of its quantitative reliability, we shall focus in Sections V E and V F on qualitative conclusions.

If  $\epsilon < 0$ , then the Ginzburg-Landau expansion of the free energy to sextic order in (74) is not bounded from below. The transition must be first

order, with higher-than-sextic order terms making the free energy bounded. In this circumstance, all we learn from (74) is that the transition is first order; we cannot obtain an estimate of the transition point or of  $\epsilon$  at the first order transition. Even though

$\epsilon$  is negative for many crystal structures [5], in all the three-flavor crystalline phases that we present in Section V D we find that  $\epsilon_{322}$  is positive and sufficiently large that  $\epsilon = 2\epsilon_{322} + 2\epsilon_{322}$  is positive. We therefore need not discuss the  $\epsilon < 0$  case any further.

## B. Two plane wave structure

We begin with the simplest three-flavor "crystal" structure in which  $f_{q_2}g$  and  $f_{q_3}g$  each contain only a single vector, yielding a condensate

$$i; j = e^{2iq_2 r} \begin{pmatrix} 2 & 2 \\ 2 & 2 \end{pmatrix} + e^{2iq_3 r} \begin{pmatrix} 3 & 3 \\ 3 & 3 \end{pmatrix}; \quad (80)$$

in which the  $u$  and  $d$  condensates are each plane waves. As explained in the previous subsection, we shall seek solutions with  $\epsilon_2 = \epsilon_3 = 0$ . We begin with such a simple ansatz both because it has been analyzed previously in Refs. [39, 41] and because it will yield a qualitative lesson which will prove extremely helpful in winnowing the space of multiple plane wave crystal structures.

Let us now walk through the evaluation of all the coefficients in the free energy (74) for this two-plane wave structure. First,  $P = 1$  (one vector in each of  $f_{q_2}g$  and  $f_{q_3}g$ ) and as always  $\epsilon$  is given by (48). Next, we obtain the results for  $\epsilon_2 = \epsilon_3$  and  $\epsilon_2 = \epsilon_3$  from the analysis of the single plane wave condensate in the two-flavor model of Ref. [35]:

$$\begin{aligned} \epsilon_2 &= \frac{1}{4} \frac{1}{\epsilon^2 - 1} = 0.569 \\ \epsilon_2 &= \frac{1}{32} \frac{\epsilon^2 + 3}{(\epsilon^2 - 1)^3} = 1.637; \end{aligned} \quad (81)$$

We now turn to  $\epsilon_{32}$  and  $\epsilon_{322}$  which describe the interaction between the  $u$  and  $d$  condensates and which we have calculated in Section V. In general,  $\epsilon_{32}$  is given by (59) but in this instance since  $f_{q_2}g$  and  $f_{q_3}g$  each contain only a single vector the sum in this equation reduces simply to

$$\epsilon_{32} = J_{32}(\theta) \quad (82)$$

where  $\theta$  is the angle between  $q_2$  and  $q_3$  and where  $J_{32}(\theta)$  is given in Eq. (58).  $\epsilon_{32}$  is plotted as a func-

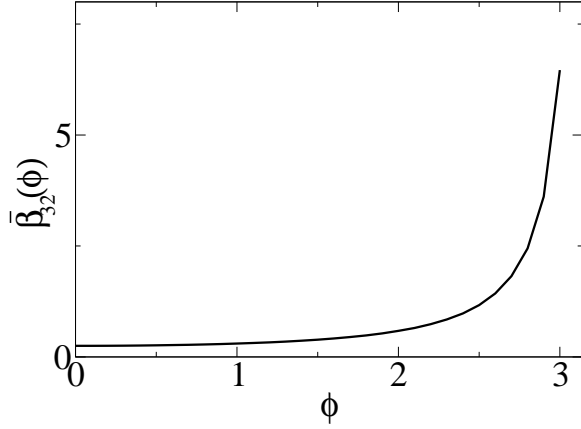


FIG. 3:  $\beta_{32}(\phi) = J_{32}(\phi)$  for the two plane wave "crystal" structure with condensate (80).  $\phi$  is the angle between  $q_2$  and  $q_3$ . For more complicated crystal structures,  $\beta_{32}$  is given by the sum in (59), meaning that it is a sum of  $J_{32}(\phi)$  evaluated at various values of  $\phi$  corresponding to the various angles between a vector in  $f_{q_2}g$  and a vector in  $f_{q_3}g$ .

tion of  $\beta_{32}$  in Fig. 3. For this simple crystal structure,  $\beta_{32}$  was calculated previously in Refs. [39, 41].

Turning to  $\beta_{322}$ , this is given by

$$\beta_{322} = \frac{3}{2} K_{322}(q_3; q_3; q_2; q_2; q_2; q_2) \quad (83)$$

where  $K_{322}$  is given by Eq. (69). As occurred in the evaluation of  $\beta_{32}$ , the sum over  $q$ -vectors in the general expression (44) has reduced to evaluating  $K_{322}$  just once, because  $f_{q_2}g$  and  $f_{q_3}g$  each contain only a single vector. For the special case where the last four arguments of  $K_{322}$  are the same, as in (83),  $K_{322}$  depends only on  $\phi$ , the angle between  $q_2$  and  $q_3$ , and the integrals in (69) can all be evaluated analytically, yielding

$$K_{322}(\phi) = \frac{1}{64 \cos^3 \frac{\phi}{2} \sin^2 \frac{\phi}{2} \sin^2 \frac{\phi}{2} \sin^2 \frac{\phi}{2} \sin^2 \frac{\phi}{2} \sin^2 \frac{\phi}{2}} \quad (84)$$

$$+ \frac{4 \sin^2 \frac{\phi}{2} \arctan(b(\phi)) \sin^2 \frac{\phi}{2}}{1 + b(\phi)^2} + \frac{b(\phi) b(\phi)^2}{(b(\phi)^2 + 1)^2} \frac{1}{5};$$

where

$$b(\phi) = \frac{\sin^2 \frac{\phi}{2} \sin^2 \frac{\phi}{2} \sin^2 \frac{\phi}{2} \sin^2 \frac{\phi}{2} \sin^2 \frac{\phi}{2} \sin^2 \frac{\phi}{2}}{\cos^3 \frac{\phi}{2}}; \quad (85)$$

$\beta_{322}$  is plotted as a function of  $\phi$  in Fig. 4.

We note that for any angle  $\phi$ , both  $\beta_{32}$  and  $2\beta_{322}$  are positive quantities which when added to the positive  $2\epsilon_0$  and  $2\epsilon_1$  give positive  $\epsilon_2$  and  $\epsilon_3$ , respectively. Hence, we see that upon making this two plane wave "crystal" structure ansatz we find a second order phase transition between the crystalline and unpaired phases, for all choices of the angle  $\phi$ . We also note that both  $\beta_{32}(\phi)$  and  $\beta_{322}(\phi)$  increase monotonically with  $\phi$ , and diverge as  $\phi \rightarrow \pi$ . This tells us that within this two plane wave ansatz, the most favorable orientation is  $\phi = 0$ , namely  $q_2 \parallel q_3$ .

Making this choice yields the smallest possible  $\epsilon_2$  and  $\epsilon_3$  within this ansatz, and hence the largest possible  $\epsilon_0$  and condensation energy, again within this ansatz. The divergence at  $\phi = \pi$  tells us that choosing  $q_2$  and  $q_3$  precisely antiparallel exacts an infinite free energy price in the combined Ginzburg-Landau and weak-coupling limit in which  $\epsilon_0 \rightarrow 0$ ;  $\epsilon_1 \rightarrow 0$ , meaning that in this limit if we chose  $\phi = \pi$  we find  $\epsilon_2 = \epsilon_3 = 0$ . Away from the Ginzburg-Landau limit, when the pairing rings on the Fermi surfaces widen into bands, choosing  $\phi = \pi$  exacts a finite price meaning that  $\epsilon_2$  is nonzero but smaller than that for any other choice of  $\phi$ . All these results confirm conclusions drawn in Refs. [39, 41] based only upon the result for  $\beta_{32}(\phi)$ .

The high cost of choosing  $q_2$  and  $q_3$  precisely an-

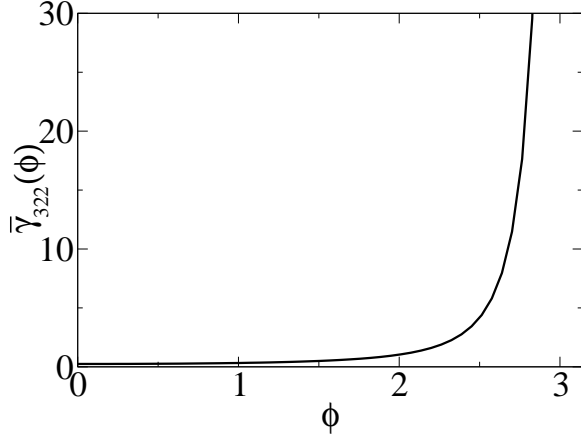


FIG. 4:  $\gamma_{322}(\phi)$  for the two plane wave "crystal" structure with condensate (80).  $\phi$  is the angle between  $q_2$  and  $q_3$ .  $\gamma_{322}(0) = 0.243$  and  $\gamma_{322}(\phi)$  increases monotonically with  $\phi$ .

tiparallel can be understood qualitatively as arising from the fact that in this case the ring of states on the u-quark Fermi surface that "want to" pair with d-quarks coincides precisely with the ring that "wants to" pair with s-quarks [41]. (For example, if  $q_2$  and  $q_3$  point in the  $-z$  and  $+z$  directions,  $\gamma_{322}(\phi)$  describes pairing between s-quarks (d-quarks) within a ring in the northern hemisphere of the s- (d-)Fermi surface and u-quarks within a ring in the southern hemisphere of the u-Fermi surface. The rings on the u-Fermi surface coincide, as illustrated in Fig. 2 of Ref. [41].) In the most favorable case within the two-plane wave ansatz, where  $q_2 \perp q_3$ , the two pairing rings on the u-quark Fermi surface are centered on antipodal points [41]. (For example, if  $q_2$  and  $q_3$  both point in the  $+z$  direction,  $\gamma_{322}(\phi)$  describes pairing of s-quarks (d-quarks) within a ring in the southern (northern) hemisphere of the s- (d-)Fermi surface and u-quarks within rings in the (northern) southern hemisphere of the u-Fermi surface.)

The simple two plane wave ansatz (80) has been analyzed in the same NJL model that we employ upon making the weak-coupling approximation but without making a Ginzburg-Landau approximation in Ref. [41]. All the qualitative lessons that we have learned from the Ginzburg-Landau approximation remain valid, including the favorability of the choice  $\phi = 0$ , but we learn further that in the two plane wave case the Ginzburg-Landau approxima-

tion always underestimates  $\gamma_{322}$  [41]. We also see from Ref. [41] that the  $\phi$  at which the Ginzburg-Landau approximation breaks down shrinks as  $\mu \rightarrow 0$ . We can understand this result as follows. The sextic term in the free energy (74) is small compared to the quartic term only if  $\mu^2 \gg \mu_e^2$ , making this a necessary condition for the quantitative validity of the Ginzburg-Landau approximation. As  $\mu \rightarrow 0$ ,  $\mu_e$  diverges more strongly than  $\mu$ : from (58) and (69) we find that as  $\mu \rightarrow 0$ ,

$$\mu_e \sim J_{32} \frac{1}{8} \frac{1}{\cos(\frac{\phi}{2})} \quad (86)$$

$$\mu_e \sim \frac{3}{2} K_{322} \frac{1}{256} \frac{1}{\cos(\frac{\phi}{2})} :$$

Therefore the Ginzburg-Landau calculation predicts that its own breakdown will occur at a  $\phi$  that decreases with increasing  $\mu$ , as found in Ref. [41] by explicit comparison with a calculation that does not employ the Ginzburg-Landau approximation.

#### C. Implications for more plane waves: qualitative principles for favorable crystal structures

In this subsection we ask what lessons we can learn from the evaluation of the Ginzburg-Landau coefficients for the two plane wave "crystal" structure in Section VIB for crystal structures with more than one vector in  $f_{q_2g}$  and  $f_{q_3g}$ .

First, we can conclude that  $\gamma_{322}$  is positive for any choice of  $f_{q_2g}$  and  $f_{q_3g}$ . The argument is simple:  $\gamma_{322}$  is given in general by (59), a sum over  $J_{32}$  evaluated at a host of angles corresponding to all angles between a vector in  $f_{q_2g}$  and  $f_{q_3g}$ . But, we see from Fig. 3 that  $J_{32}$  is positive at any angle.

Second, we cannot draw a conclusion about  $\gamma_{322}$ . This coefficient is a sum over contributions of the form  $K_{322}(q_3^b; q_3^b; q_2^d; q_2^e; q_2^f; q_2^a)$  where the last four momentum vector arguments, selected from  $f_{q_2g}$ , must satisfy (62). The calculation in Section VIB whose result is plotted in Fig. 4 only demonstrates that those contributions in which the four  $q_3$  arguments are selected to all be the same vector are positive. For any crystal structure in which  $f_{q_2g}$  contains two or more vectors, there are other contributions to  $\gamma_{322}$  that we have not evaluated in

this section which depend on one  $q_2$  vector and several  $q_3$  vectors, and thus on more than one angle. We know of instances where individual contributions  $K_{322}(q_3^b; q_3^b; q_2^d; q_2^e; q_2^f; q_2^a)$  in crystal structures that we describe below are negative. However, we have found no crystal structure for which  $\epsilon_{322}$  is negative.

The main lesson we learn is that crystal structures in which any of the vectors in  $fq_2g$  are close to antiparallel to any of the vectors in  $fq_3g$  are strongly disfavored. (The closer to antiparallel, the worse, with the free energy penalty for  $\epsilon \neq 0$  diverging for the precisely antiparallel case, driving to zero.) If a vector in  $fq_2g$  is antiparallel (or close to antiparallel) to one in  $fq_3g$ , this yields in  $\epsilon_{32}$  (or merely large) positive contributions to  $\epsilon_{32}$  and to  $\epsilon_{322}$  and hence to  $\epsilon_e$  and  $\epsilon_e$ . In the case of  $\epsilon_{32}$ , these large positive contributions cannot be cancelled since all contributions are positive. In the case of  $\epsilon_{322}$ , negative contributions are possible but we know of no instances of divergent negative contributions to  $\epsilon_{322}$  or indeed to any other coefficient in the Ginzburg-Landau expansion. The divergent positive contributions are associated with the tangential intersection (in the case of  $\epsilon_{32}$  and  $\epsilon_{32}$ ) or coincidence (in the case of  $\epsilon_{32}$  and  $\epsilon_{322}$ ) of pairing rings on Fermi surfaces. We know of no configuration of rings that leads to an infinitely favorable (as opposed to unfavorable) free energy in the combined Ginzburg-Landau and weak-coupling limits. So, although we do not have a proof that the divergent positive contributions to  $\epsilon_{322}$  arising as vectors in  $fq_2g$  and  $fq_3g$  approach one another's antipodes are uncanceled, we also see no physical argument for how this could conceivably arise. Certainly in all example crystal structures that we have considered,  $\epsilon_{32}$  and  $\epsilon_{322}$  and hence  $\epsilon_e$  and  $\epsilon_e$  diverge as vectors in  $fq_2g$  and  $fq_3g$  approach one another's antipodes.

We can now summarize the qualitative principles that we have arrived at for constructing favorable crystal structures for three-flavor crystalline color superconductivity. First, as described in Section III the sets  $fq_2g$  and  $fq_3g$  should each separately be chosen to yield crystal structures which, seen as separate two-flavor crystalline phases, are as favorable as possible. In Section III we have reviewed the results of Ref. [35] for how this should be done, and the conclusion that the most favored  $fq_2g$  or  $fq_3g$  in isolation consists of eight vectors pointing at the corners of a cube. Second, the new addition in the three-flavor case is the qualitative principle that  $fq_2g$  and  $fq_3g$  should be rotated with respect

to each other in such a way as to best keep vectors in one set away from the antipodes of vectors in the other set.

#### D. Multiple plane waves

In Table I we describe 11 different crystal structures that we have analyzed, and in Table II we give the coefficients that specify each Ginzburg-Landau free energy (72). The  $\epsilon_{32}$ 's and  $\epsilon_{322}$ 's were calculated as described in Ref. [35];  $\epsilon_{32}$ 's and  $\epsilon_{322}$ 's were calculated as described in Section V. We also give the combinations  $\epsilon_e$  and  $\epsilon_e$  defined in (74) that specify the free energy as in (75). In those cases in which  $\epsilon_e < 0$ , the phase transition between the crystalline phase and the unpaired phase is first order, occurring where  $\epsilon_e = 0$  with  $\epsilon_e$  given by (78). At the first order phase transition, unpaired quark matter with  $\epsilon_e = 0$  and crystalline quark matter with  $\epsilon_e = 0$  given in (79) have the same free energy. We give both  $\epsilon_e$  and  $\epsilon_e$  in Table II.

The first row of the Tables describes the simple "crystal structure" analyzed in detail in Section VIB, in which both  $fq_2g$  and  $fq_3g$  contain just a single vector, with  $q_2 \perp q_3$  as we have seen that this is the most favorable choice for the angle between  $q_2$  and  $q_3$ . This condensate carries a baryon number current which means that the unpaired gapless fermions (in "blocking regions" in momentum space [30, 31]) must carry a current that is equal in magnitude but opposite in direction [30]. The analysis of this "crystal structure" in Sections VIB and VIC has proved instructive, giving us qualitative insight that we shall use to understand all the other crystal structures. However, in all rows in the Tables other than the first we have chosen crystal structures with condensates that carry no net current, meaning that the gapless fermions need carry no current. There is nothing in our mean-field analysis that precludes condensates carrying a net current, but we do not analyze them here primarily because it simplifies our task but also because we expect that, beyond mean-field theory, a phase containing gapless fermions carrying a net current is unlikely to be the favored ground state.

Let us next examine the last two rows of the Tables. Here, we consider two crystal structures in which  $fq_2g$  and  $fq_3g$  each contain eight vectors forming cubes. Since the cube is the most favorable two-flavor crystal structure according to the analy-

Structure	Description	Largest Angle
2PW	$f_{q_2}g$ and $f_{q_3}g$ coincide; each contains one vector. (So, 2 plane waves with $q_2 \parallel q_3$ .)	0
SqX	$f_{q_2}g$ and $f_{q_3}g$ each contain two antiparallel vectors. The four vectors together form a square; those from $f_{q_2}g$ and those from $f_{q_3}g$ each form one stroke of an "X".	90
Tetrahedron	$f_{q_2}g$ and $f_{q_3}g$ each contain two vectors. The four together form a tetrahedron.	109.5
2Triangles	$f_{q_2}g$ and $f_{q_3}g$ coincide; each contains three vectors forming a triangle.	120
Cube X See Eq. (90)	$f_{q_2}g$ and $f_{q_3}g$ each contain 4 vectors forming a rectangle. The 8 vectors together form a cube. The 2 rectangles intersect to look like an "X" if viewed end-on.	109.5
2Tet	$f_{q_2}g$ and $f_{q_3}g$ coincide; each contains four vectors forming a tetrahedron.	109.5
Twisted Cube	$f_{q_2}g$ and $f_{q_3}g$ each contain four vectors forming a square which could be one face of a cube. Instead, the eight vectors together form the polyhedron obtained by twisting the top face of a cube by 45° relative to its bottom face.	143.6
20cta90xy	$f_{q_2}g$ and $f_{q_3}g$ each contain 6 vectors forming an octahedron. The $f_{q_2}g$ vectors point along the positive and negative axes. The $f_{q_3}g$ -octahedron is rotated relative to the $f_{q_2}g$ -octahedron by 90° about the (1;1;0)-axis.	135
20cta45xyz	$f_{q_2}g$ and $f_{q_3}g$ each contain 6 vectors forming an octahedron. The $f_{q_2}g$ vectors point along the positive and negative axes. The $f_{q_3}g$ -octahedron is rotated relative to the $f_{q_2}g$ -octahedron by 45° about the (1;1;1)-axis.	143.6
2Cube45z See Eq. (87)	$f_{q_2}g$ and $f_{q_3}g$ each contain 8 vectors forming a cube. The $f_{q_2}g$ vectors point along (1; 1; 1). The $f_{q_3}g$ -cube is rotated relative to that by 45° about the z-axis.	143.6
2Cube45xy	$f_{q_2}g$ and $f_{q_3}g$ each contain 8 vectors forming a cube. The $f_{q_2}g$ vectors point along (1; 1; 1). The $f_{q_3}g$ -cube is rotated relative to that by 45° about the (1;1;0)-axis.	154.5

TABLE I: Descriptions of the crystal structures whose Ginzburg-Landau coefficients are given in Table II. The third column is the largest angle between any vector in  $f_{q_2}g$  and any vector in  $f_{q_3}g$ . Other things being equal, we expect that the larger the largest angle, meaning the closer vector(s) in  $f_{q_2}g$  get to vector(s) in  $f_{q_3}g$ , the bigger the  $\kappa_{32}$  and hence the bigger the  $\epsilon_e$  and  $\epsilon_{\text{eff}}$ , and hence the less favorable the structure.

Structure	$\kappa_{32}$	$\epsilon_e$	$\epsilon_{\text{eff}}$	$\kappa_{32}$	$\epsilon_e$	$\epsilon_{\text{eff}}$	$\kappa_{32}$	$\epsilon_e$	$\epsilon_{\text{eff}}$
2PW	0.569	0.250	1.388	1.637	0.243	3.760	0	0	0
SqX	0.138	1.629	1.906	1.952	2.66	9.22	0	0	0
Tetrahedron	-0.196	2.146	1.755	1.450	7.21	17.29	0	0	0
2Triangles	-1.976	4.647	0.696	1.687	13.21	29.80	0	0	0
CubeX	-10.981	6.961	-15.001	-1.018	19.90	37.76	0.140	0.548	0.548
2Tet	-5.727	7.439	-4.015	4.350	30.35	69.40	0.0054	0.208	0.208
Twisted Cube	-16.271	12.445	-20.096	-37.085	315.5	556.8	0.0170	0.165	0.165
20cta90xy	-31.466	18.665	-44.269	19.711	276.9	593.2	0.0516	0.237	0.237
20cta45xyz	-31.466	19.651	-43.282	19.711	297.7	634.9	0.0461	0.226	0.226
2Cube45z	-110.757	36.413	-185.101	-459.24	1106.	1294.	0.310	0.328	0.328
2Cube45xy	-110.757	35.904	-185.609	-459.24	1135.8	2179.8	0.0185	0.0799	0.0799

TABLE II: Ginzburg-Landau coefficients for three-flavor crystalline color superconducting phases with various crystal structures, described in Table I.  $\kappa_{32}$  is the  $\kappa$  at which the transition from unpaired quark matter to a given crystalline phase occurs:  $\kappa_{32} = 0$  if  $\epsilon_e > 0$  and the transition is second order;  $\kappa_{32}$  is given by (78) if  $\epsilon_e < 0$  and the transition is first order. For a first order transition,  $\epsilon_{\text{eff}}$  ( ), given in (79), is the magnitude of the gap at the transition.



sis of Ref. [35], evident in the large negative  $\epsilon$  and  $\epsilon_e$  for both these crystal structures in Table II, this should be a good starting point. We cannot have the two cubes coincident, as in that case there are vectors from  $fq_2g$  and vectors from  $fq_3g$  separated by a  $180^\circ$  angle, yielding in nite positive contributions to both  $\epsilon_{32}$  and  $\epsilon_{322}$ . So, we rotate the  $fq_3g$ -cube relative to the  $fq_2g$  cube, in two different ways in the 2Cube45z and 2Cube45xy crystal structures described in Table I.

We explain explicitly in Appendix B why translating one cube relative to the other in position space by a fraction of a lattice spacing does not alleviate the problem: a relative rotation of the h<sub>u</sub>si and h<sub>u</sub>di condensates is required. Qualitatively, this reflects the nature of the difficulty that occurs when a  $fq_2g$  vector is opposite to a  $fq_3g$  vector. It can be thought of as arising because the h<sub>u</sub>si and h<sub>u</sub>di condensates both want to "use" those up quarks lying on the same ring on the up Fermi surface. It therefore makes sense that a relative rotation is required. Quantitatively, what we show in Appendix B is that  $\epsilon$  does not change if we translate the h<sub>u</sub>si condensate relative to the h<sub>u</sub>di condensate.

We see in Table I that in the 2Cube45z structure, the largest angle between vectors in  $fq_2g$  and  $fq_3g$  is  $143.6^\circ$  whereas in the 2Cube45xy structure, that largest angle is  $154.5^\circ$  meaning that the rotation we have chosen does a less good job of keeping  $fq_2g$ -vectors away from the antipodes of  $fq_3g$  vectors. Correspondingly, we see in Table II that 2Cube45xy has a much larger  $\epsilon_{322}$  and hence  $\epsilon_e$ , and hence has a first order phase transition occurring at a smaller  $\mu$  and with a smaller  $\mu_c$ . This is an example confirming our general principle that, other things being equal, crystal structures in which  $fq_3g$  vectors come closer to  $fq_2g$  vectors will be disfavored. According to this principle, the 2Cube45z crystal structure should be particularly favorable as it employs the relative rotation between the two cubes that does the best possible job of keeping them apart.

We now turn to crystal structures with fewer than 16 plane waves. By having fewer than 8 plane waves in  $fq_2g$  and  $fq_3g$ , we are no longer optimizing the two-avor and  $\epsilon_e$ . However, with fewer vectors it is possible to keep the  $fq_2g$ - and  $fq_3g$ -vectors farther away from each other's antipodes. We list two crystal structures in which  $fq_2g$  and  $fq_3g$  have 6 waves forming octahedra. These are not particularly favorable two-avor structures |  $\epsilon$  is positive rather than being large and negative for the cube. 2Octa45xyz

has the same largest angle between  $fq_2g$ - and  $fq_3g$ -vectors as 2Cube45z, but its significantly more positive  $\epsilon$  and  $\epsilon_e$  make it significantly less favorable. Choosing the 2Octa90xy structure instead reduces the largest angle between  $fq_2g$ - and  $fq_3g$ -vectors from  $143.6^\circ$  to  $135^\circ$ , which improves  $\epsilon_e$  and  $\epsilon_e$ , but only slightly.

We investigate three crystal structures in which  $fq_2g$  and  $fq_3g$  each contain 4 vectors. Among these, the Twisted Cube is strongly disfavored by its significantly larger largest angle between  $fq_2g$ - and  $fq_3g$ -vectors. CubeX and 2Tet are both constructed by choosing  $fq_2g$  and  $fq_3g$  as subsets containing half the vectors from a cube. In the 2Tet structure, we choose the tetrahedra coincident since this does the best job of keeping vectors in  $fq_2g$  and  $fq_3g$  away from each other's antipodes. (Choosing the two tetrahedra so that their union forms a cube is the worst possible choice, as vectors in  $fq_2g$  and  $fq_3g$  are then antipodal.) In the CubeX structure, we choose the two rectangles such that their union forms a cube, as this does the best job of reducing the largest angle between vectors in  $fq_2g$  and  $fq_3g$ ; making the rectangles coincident would have been the worst possible choice. CubeX and 2Tet have the same largest angle, but they differ considerably in that the  $fq_2g$  and  $fq_3g$  rectangles that make up CubeX are more favorable two-avor structures (lower  $\epsilon$  and  $\epsilon_e$ ) than the tetrahedra that make up 2Tet. We see from Table II that the CubeX structure, with only 8 vectors in total, is particularly favorable: it is not possible to tell from Table II whether it is more or less favorable than 2Cube45z, since one has the larger  $\epsilon$  while the other has the larger  $\epsilon_e$ . We shall evaluate their free energies below, and confirm that they are indeed comparable, and that these two structures have the lowest free energy of any in the Tables.

In the remaining rows of the Tables, we investigate one crystal structure in which  $fq_2g$  and  $fq_3g$  each contain 3 vectors, and two in which each contain 2 vectors. These structures all have positive  $\epsilon_e$ , and hence second order phase transitions, and so are certainly not favored.

Inspecting the results in Table II shows that in all cases where we have investigated different three-avor crystal structures built from the same  $fq_2g$  and  $fq_3g$ , the one with the relative rotation between the two polyhedra that yields the smaller largest angle between vectors in  $fq_2g$  and  $fq_3g$  is favored. And, in all cases where we have investi-

gated two crystal structures with same largest angle between vectors in  $f_{q_2}g$  and  $f_{q_3}g$ , the one built from the more favorable two-avor crystal structure is favored. We thus find no exceptions to the qualitative principles we described in Section V I C . However, these qualitative principles certainly do not explain all the features of the results in Table II. For example, we have no qualitative understanding of why 2Cube45z and 2Cube45xy have such similar  $\beta_{32}$ , whereas 2Cube45xy has a much larger  $\beta_{32}$  as expected. For example, we have no qualitative understanding of why  $\beta_{32}$  increases much more in going from 2Cube45xy to 2Cube45z than it does in going from 2Octa90xy to 2Octa45xyz. The calculations must be done; the qualitative principles are a good guide, but not a substitute.

The final crystal structure that we describe is one in which  $f_{q_2}g$  is a cube while  $f_{q_3}g$  is an octahedron, with the six  $f_{q_3}g$ -vectors pointing at the centers of the faces of the  $f_{q_2}g$ -cube. So, if the  $f_{q_2}g$ -vectors are taken to point along the  $(1; 1; 1)$  directions then the  $f_{q_3}g$  vectors point along the positive and negative axes. We chose to investigate this structure because it seems particularly symmetric and because it has an unusually small largest angle between vectors in  $f_{q_2}g$  and  $f_{q_3}g$  given the large number of vectors in total: 125:3. Because  $f_{q_2}g$  and  $f_{q_3}g$  are not congruent,  $\beta_{23} \neq \beta_{32}$  and  $\beta_{23} \neq \beta_{31}$ . All these coefficients can be found in Table II. We find  $\beta_{32} = 24.510$ ,  $\beta_{22} = 419.9$  and  $\beta_{233} = 4943$ : Because  $f_{q_2}g$  and  $f_{q_3}g$  are not exchange symmetric, the general argument that we gave in Section V I A for why extrema of  $(\beta_{22}; \beta_{33})$  i.e. solutions to the gap equations | occur at  $\beta_{22} = \beta_{33}$  does not apply. However, we find that at the solution  $\beta_{22}$  and  $\beta_{33}$  differ by less than 20%. The large values of  $\beta_{233}$  and  $\beta_{322}$  make this crystal structure quite unfavorable | even though it has a (weak) first order phase transition, its free energy turns out to be comparable only to that of the 2PW structure, far above the free energy of the favored CubeX and 2Cube45z structures. Furthermore, the arguments of Appendix A do not apply to a crystal structure like this, meaning that we do not expect this solution with  $\beta_{22} \neq \beta_{33}$  to be neutral. For this reason, and because it appears to be free-energetically unfavorable anyway, we will not investigate it further. We cannot say whether choosing  $f_{q_2}g$  and  $f_{q_3}g$  to not be exchange symmetric generically yields an unfavorable crystal structure, as we have not investigated many possibilities.

We have certainly not done an exhaustive search

of three-avor crystal structures. For example, we have only scratched the surface in investigating structures in which  $f_{q_2}g$  and  $f_{q_3}g$  are not exchange symmetric. We have investigated the structures that are the best that we can think of according to the qualitative principles described in Section V I C . Readers should feel free to try others. (We are confident that in 2Cube45z we have found the most favorable structure obtained by rotating one cube relative to another. We are not as confident that CubeX is the best possible structure with fewer than  $8+8$  vectors.) As we shall see in Section V I E , however, the two most favorable structures that we have found, 2Cube45z and CubeX, are impressively robust and do a very good job of making the case that three-avor crystalline color superconducting phases are the ground state of cold quark matter over a wide range of densities. If even better crystal structures can be found, this will only further strengthen this case.

#### E. Free energy comparisons

We can now evaluate and plot the gap parameter and free energy  $(\epsilon)$  for all the crystal structures described in Table I, whose Ginzburg-Landau coefficients are given in Table II. For a given crystal structure,  $(\epsilon)$  is given by Eq. (74), with  $\epsilon_e$  and  $\epsilon_s$  taken from Table II. The quadratic coefficient is related to  $\beta_{22}$  by Eq. (8). Recall that we have made the approximation that  $\beta_{22} = \beta_{33} = \beta_{233} = M_s^2 = (8)$ , valid up to corrections of order  $M_s^3 = 4$ . At any value of  $M_s^2$ , we can evaluate  $(\epsilon)$  and hence  $(\epsilon)$ , determine  $\beta_{22}$  by minimizing  $(\epsilon)$ , and finally evaluate the free energy  $\epsilon$  at the minimum. In Fig. 5, we give an example of  $(\epsilon)$  for various  $M_s^2$  for one crystal structure with a first order phase transition (CubeX), illustrating how the first order phase transition is found, and how the solving the gap equations | i.e. minimizing  $(\epsilon)$  is found. We plot  $\epsilon$  and  $\beta_{22}$  at the minimum versus  $M_s^2$  in Figs. 6 and 7 for some of the crystal structures in Tables I and II.

In Figs. 6 and 7, we show two examples of crystal structures for which the phase transition to the unpaired state is second order: 2PW and SqX. (See Table I for descriptions of these structures.) The second order phase transition occurs at  $M_s^2 = 7.60$   $\mu_0 = 190.0$  MeV, where  $\epsilon = 0$ . (See Eq. (76).) We show four examples of crystal structures with

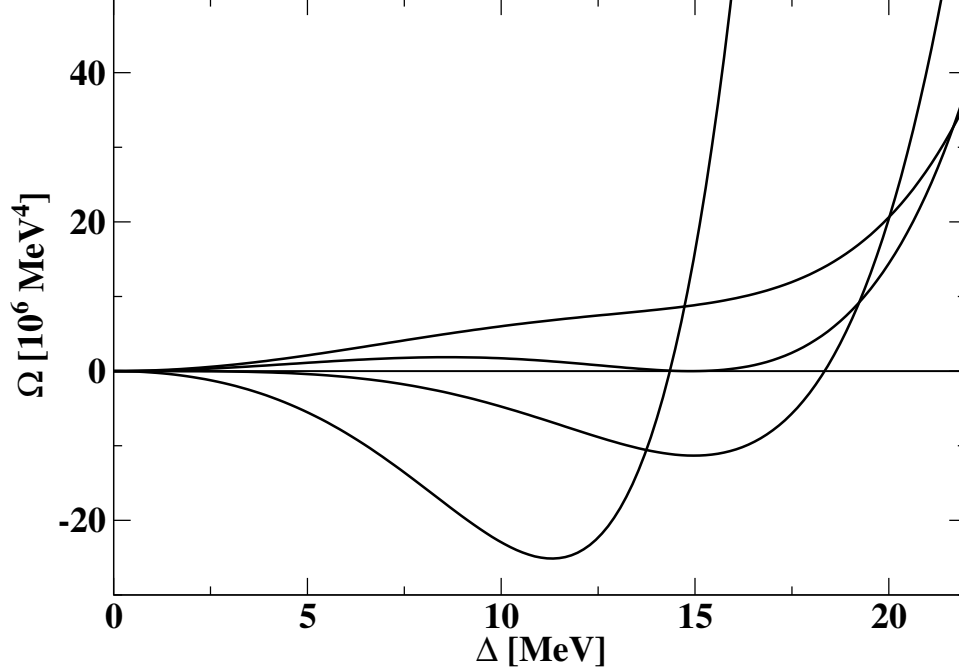


FIG. 5: Free energy  $\Omega$  vs.  $\Delta$  for the CubeX crystal structure, described in Table II, at four values of  $M_s^2 =$ . From top curve to bottom curve, as judged from the left half of the figure, the curves are  $M_s^2 = 240, 218.61, 190$ , and  $120$  MeV, corresponding to  $\alpha = 0.233, 0.140, 0, -0.460$ . The first order phase transition occurs at  $M_s^2 = 218.61$  MeV. The values of  $\Delta$  and  $\Omega$  at the minima of curves like these are what we plot in Figs. 6 and 7.

first order phase transitions, occurring where  $\Omega = 0$  and  $\Delta > 0$  meaning at some  $M_s^2 > 190.0$  MeV. We show the two most favorable structures that we have found: CubeX and 2Cube45z. And, we show two examples (2Tet and 2Octa90xy) of structures with first order phase transitions that are more favorable than the structures with a second order transition, but less favorable than CubeX and 2Cube45z.

In Figs. 6 and 7, we have chosen the interaction strength between quarks such that the CFL gap parameter at  $M_s = 0$  is  $\mu_0 = 25$  MeV. However, our results for both the gap parameters and the condensation energy for any of the crystalline phases can easily be scaled to any value of  $\mu_0$ . We saw in Section V that the quartic and sextic coefficients in the Ginzburg-Landau free energy do not depend on  $\mu_0$ . And, recall from Eq. (48) that  $\mu_0$  enters only through the combination  $\mu_{2SC} = \mu_0$ , where  $\mu_{2SC} = 2^{\frac{1}{3}} \mu_0$  and  $\mu_s = M_s^2 = (8 \mu_0^2)$ . This means that if we pick a  $\mu_0 \neq 25$  MeV, the curves describing the gap parameters for the crystalline phases in Fig. 6 are precisely unchanged if we rescale both the verti-

cal and horizontal axes proportional to  $\mu_0 = 25$  MeV. In the case of Fig. 7, the vertical axis must be rescaled by  $(\mu_0 = 25 \text{ MeV})^2$ . Of course, the weak-coupling approximation  $\mu_0 \ll \Lambda$ , which we have used for example in simplifying the propagators in (52), will break down if we scale  $\mu_0$  to be too large. We cannot evaluate up to what  $\mu_0$  we can scale our results reliably without doing a calculation that goes beyond the weak-coupling limit. However, such calculations have been done for the gCFL phase in Ref. [15], where it turns out that the gaps and condensation energies plotted Figs. 6 and 7 scale with  $\mu_0$  and  $\mu_0^2$  to good accuracy for  $\mu_0 \leq 40$  MeV with  $\Lambda = 500$  MeV, but the scaling is significantly less accurate for  $\mu_0 = 100$  MeV. Of course, for  $\mu_0$  as large as 100 MeV, any quark matter in a compact star is likely to be in the CFL phase. Less symmetrically paired quark matter, which our results suggest is in a crystalline color superconducting phase, will occur in compact stars only if  $\mu_0$  is smaller, in the range where our results can be expected to scale well.

The qualitative behavior of  $\Omega$  at smaller  $M_s^2 =$ , well to the left of the unpaired/crystalline phase

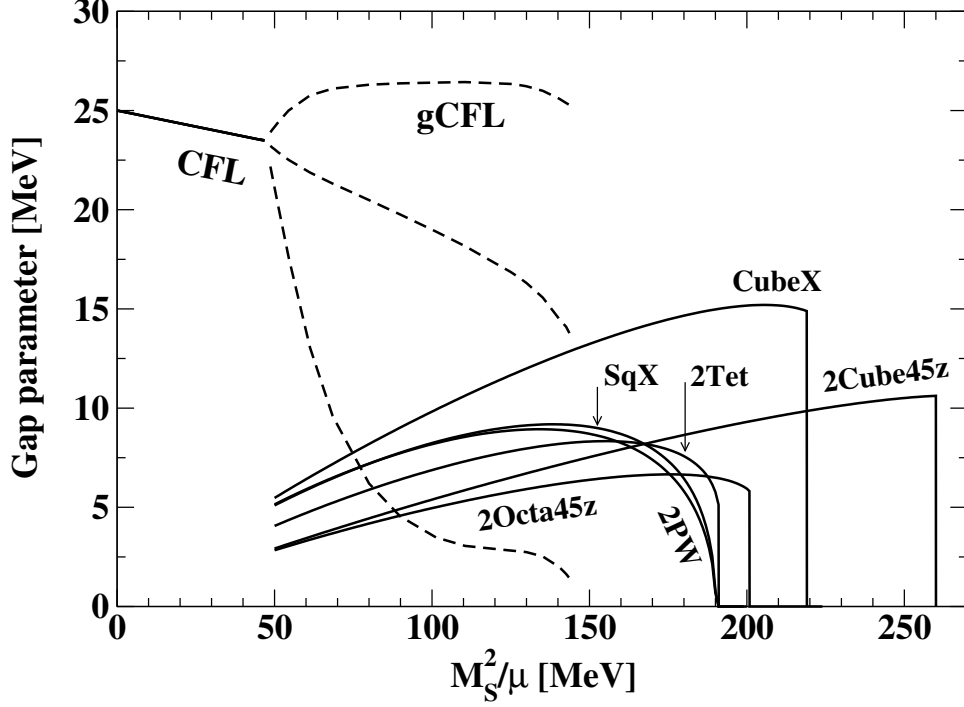


FIG. 6: Gap parameter versus  $M_s^2/\mu$  for three-flavor crystalline color superconducting phases with various crystal structures. The crystal structures are described in Table II. For comparison, we also show the CFL gap parameter and the gCFL gap parameters  $\Delta_1$ ,  $\Delta_2$  and  $\Delta_3$  [11, 12]. Recall that the splitting between Fermi surfaces is proportional to  $M_s^2/\mu$ , and that small (large)  $M_s^2/\mu$  corresponds to high (low) density.

transitions in Fig. 6, can easily be understood. The quadratic, quartic and sextic coefficients in the free energy (74) are  $\propto \mu^{-1}$ ,  $\propto \mu^{-2}$  and  $\propto \mu^{-3}$ . If  $\mu$  tended to a constant at small  $M_s^2/\mu$ , then the solution  $m_{\min}$  that minimizes would be proportional to  $\mu^{-1/2}$ . (See Eq. (77).) In fact, from (48) we see that  $\mu/\log \mu$  at small  $\mu$ , meaning that, according to (77),  $m_{\min}$  should vanish slightly more slowly than linear as  $M_s^2/\mu \rightarrow 0$ , as in Fig. 6. And, since the  $\mu$ 's vanish for  $M_s^2/\mu \rightarrow 0$ , so do the condensation energies of Fig. 7.

Fig. 6 can be used to evaluate the validity of the Ginzburg-Landau approximation. The simplest criterion is to compare the  $\mu$ 's for the crystalline phases to the CFL gap parameter  $\Delta_0$ . This is the correct criterion in the vicinity of the 2nd order phase transition point, where  $\mu = M_s^2/(8\pi^2)$ . Well to the left, it is more appropriate to compare the  $\mu$ 's for the crystalline phase to  $\mu = M_s^2/(8\pi^2)$ . By either criterion, we see that all the crystal structures with first order phase transitions (including the

two that are most favored) have  $\mu$ 's that are large enough that the Ginzburg-Landau approximation is at the edge of its domain of validity, a result which we expected based on the general arguments in Section V I A. Note that the Ginzburg-Landau approximation is controlled for those structures with second order phase transitions only near the second order phase transition, again a result that can be argued for on general grounds.

Fig. 7 makes manifest one of the central conclusions of our work. The three-flavor crystalline color superconducting phases with the two most favored crystal structures that we have found are robust by any measure. Their condensation energies reach about half that of the CFL phase at  $M_s = 0$ , remarkable given that in the CFL phase pairing occurs over the whole of all three Fermi surfaces. Correspondingly, these two crystal structures are favored over the wide range of  $M_s^2/\mu$  seen in Fig. 7 and given in Eq. (2).

Taken literally, Fig. 7 indicates that within the

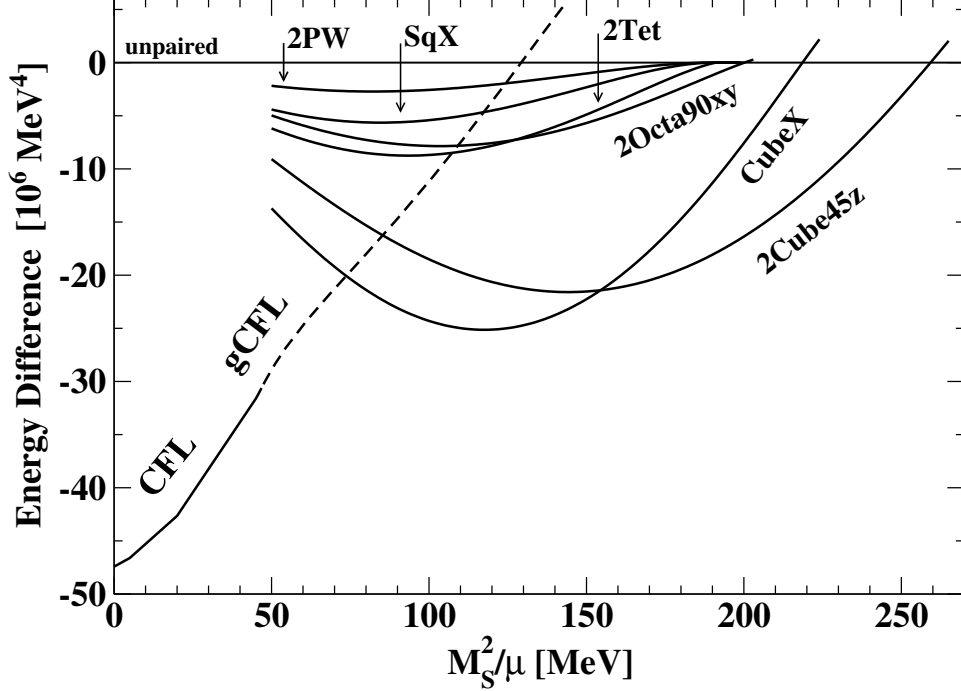


FIG. 7: Free energy versus  $M_s^2/\mu$  for the three-flavor crystalline color superconducting phases with various crystal structures whose gap parameters are plotted in Fig. 6. The crystal structures are described in Table II. Recall that the gCFL phase is known to be unstable, meaning that in the regime where the gCFL phase free energy is plotted, the true ground state of three-flavor quark matter must be some phase whose free energy lies below the dashed line. We see that the three-flavor crystalline color superconducting quark matter phases with the most favorable crystal structures that we have found, namely 2Cube45z and CubeX described in (87) and (90), have sufficiently robust condensation energy (sufficiently negative) that they are candidates to be the ground state of three-flavor quark matter over a wide swath of  $M_s^2/\mu$ , meaning over a wide range of densities.

regime (2) of the phase diagram occupied by crystalline color superconducting quark matter, the 2Cube45z phase is favored at lower densities and the CubeX phase is favored at higher densities. Although, as detailed in Sections VIC and VID, we do have qualitative arguments why 2Cube45z and CubeX are favored over other phases, we have no qualitative argument why one should be favored over the other. And, we do not trust that the Ginzburg-Landau approximation is sufficiently quantitatively reliable to trust the conclusion that one phase is favored at higher densities while the other is favored at lower ones. We would rather leave the reader with the conclusion that these are the two most favorable phases we have found, that both are robust, that the crystalline color superconducting phase of three-flavor quark matter with one crystal structure or the other occupies a wide swath of the QCD phase dia-

gram, and that their free energies are similar enough to each other that it will take a beyond-Ginzburg-Landau calculation to compare them reliably.

## VII. CONCLUSIONS, IMPLICATIONS, AND FUTURE WORK

We have evaluated the gap parameter and free energy for three-flavor quark matter in crystalline color superconducting phases with varied crystal structures, within a Ginzburg-Landau approximation. Our central results are shown in Figs. 6 and 7. Descriptions of the crystal structures that we have investigated, together with the coefficients for the Ginzburg-Landau free energy (74) for each structure, are given in Tables I and II.

We have found two qualitative rules that guide our

understanding of what crystal structures are favored in three-avor crystalline quark matter. First, the hudi and husi condensates separately should be chosen to have favorable free energies, as evaluated in the two-avor model of Ref. [35]. Second, the hudi and husi condensates should be rotated relative to each other in such a way as to maximize the angles between the wave vectors describing the crystal structure of the hudi condensate and the antipodes of the wave vectors describing the husi condensate. This second qualitative rule can be understood as minimizing the "competition" between the two condensates for up quarks on the up Fermi surface, as first elucidated in a simpler setting in Ref. [41].

Fig. 7 shows that over most of the range of  $M_s^2 =$  where it was once considered a possibility, the gCFL phase can be replaced by a much more favorable three-avor crystalline color superconducting phase. However, Fig. 7 also indicates that it is hard to find a crystal structure which yields a crystalline phase that has lower free energy than the gCFL phase at the lowest values of  $M_s^2 =$  (highest densities) in the "gCFL window", closest to the CFL! gCFL transition. This narrow window where the gCFL curve remains the lowest curve in Fig. 7 is therefore the most likely place in the QCD phase diagram in which to find the gCFL phase augmented by current-carrying meson condensates described in Refs. [45, 46]. Except within this window, the crystalline color superconducting phases with either the CubeX or the 2Cube45z crystal structure provide an attractive resolution to the instability of the gCFL phase.

The three-avor crystalline color superconducting phases with the CubeX and 2Cube45z crystal structures have condensation energies that can be as large as half that of the CFL phase. This robustness makes them the lowest free energy phase that we know of, and hence a candidate for the ground state of QCD, over a wide range of densities. To give a

sense of the implications of the range of  $M_s^2 =$  over which crystalline color superconductivity is favored, given by Eq. (2) and shown in Fig. 7, if we suppose that  $\mu_0 = 25$  MeV and  $M_s = 250$  MeV, the window (2) translates to  $240 \text{ MeV} < < 847 \text{ MeV}$ . With these choices of parameters, then, the lower part of this range of (higher part of the range of  $M_s^2 =$ ) is certainly superseded by nuclear matter. And, the high end of this range extends far beyond the 500 MeV characteristic of the quark matter at the densities expected at the very center of compact stars. Our result therefore suggests that if compact stars have quark matter cores, it is entirely reasonable to suppose that the entire quark matter core could be in a crystalline color superconducting phase. Of course, if  $\mu_0$  is larger, say 100 MeV, the entire quark matter core could be in the CFL phase. And, there are reasonable values of  $\mu_0$  and  $M_s$  for which the outer layer of a possible quark matter core would be in a crystalline phase while the inner core would not. We do not know  $\mu_0$  and  $M_s$  well enough to answer the question of what phases of quark matter occur in compact stars. However, our results add the possibility that as much as all of the quark matter in a compact star could be in a crystalline color superconducting phase to the menu of options that must ultimately be winnowed by confrontation with astrophysical observations.

We have identified two particularly favorable crystal structures, using the qualitative rules described above and by direct calculation. We do not believe that our Ginzburg-Landau approximation is sufficiently accurate to trust its determination of which of these two structures is more favorable. For this reason, we wish to leave the reader with a picture of both the 2Cube45z and CubeX crystal structures in position space. In the 2Cube45z phase, the color-avor and position space dependence of the condensate, defined in (20) and (21), is given by



$$\begin{aligned}
\psi_{CF}(\mathbf{x})_{ij} = & \frac{1}{2} \left[ \cos \frac{2\pi}{a} (x+y+z) + \cos \frac{2\pi}{a} (x-y+z) \right. \\
& + \cos \frac{2\pi}{a} (x+y-z) + \cos \frac{2\pi}{a} (x-y-z) \\
& + \frac{1}{3} \left[ \cos \frac{2\pi}{a} \left( \frac{p}{2}x + z \right) + \cos \frac{2\pi}{a} \left( \frac{p}{2}y + z \right) \right. \\
& \left. \left. + \cos \frac{2\pi}{a} \left( \frac{p}{2}y + z \right) + \cos \frac{2\pi}{a} \left( \frac{p}{2}x + z \right) \right] \right];
\end{aligned} \tag{87}$$

where  $\mathbf{x}$  and  $(i, j)$  are color (flavor) indices and where

$$a = \frac{p}{q} = \frac{4.536}{1.764 M_s^2} \tag{88}$$

is the lattice spacing of the face-centered cubic crystal structure. For example, with  $M_s^2 = 100; 150; 200$  MeV the lattice spacing is  $a = 72; 48; 36$  fm. Eq. (87) can equivalently be written as

$$\psi_{CF}(\mathbf{x})_{ij} = \frac{1}{2} \left[ \psi_2(\mathbf{r}) + \psi_3(\mathbf{r}) \right]; \tag{89}$$

with (87) providing the expressions for  $\psi_2(\mathbf{r})$  and  $\psi_3(\mathbf{r})$ . A three-dimensional contour plot that can be

seen as depicting either  $\psi_2(\mathbf{r})$  or  $\psi_3(\mathbf{r})$  separately can be found in Ref. [35]. We have not found an informative way of depicting the entire condensate in a single contour plot. Note also that in (87) and below in our description of the CubeX phase, we make an arbitrary choice for the relative position of  $\psi_3(\mathbf{r})$  and  $\psi_2(\mathbf{r})$ . We show in Appendix B that one can be translated relative to the other at no cost in free energy. Of course, as we have investigated in detail in Section VI, rotating one relative to the other changes the Ginzburg-Landau coefficients  $\kappa_{32}$  and  $\kappa_{22}$  and hence the free energy.

In the CubeX phase, the color-flavor and position space dependence of the condensate is given by

$$\begin{aligned}
\psi_{CF}(\mathbf{x})_{ij} = & \frac{1}{2} \left[ \cos \frac{2\pi}{a} (x+y+z) + \cos \frac{2\pi}{a} (x-y+z) \right. \\
& + \frac{1}{3} \left[ \cos \frac{2\pi}{a} (x+y+z) + \cos \frac{2\pi}{a} (x-y+z) \right] \right];
\end{aligned} \tag{90}$$

We provide a depiction of this condensate in Fig. 8.

The gap parameter is large enough in both the 2Cube45z and CubeX phases that the Ginzburg-Landau approximation that we have used to obtain our results is being pushed to the limits of its validity. Therefore, although we expect that the qualitative lessons that we have learned about the favorabil-

ity of crystalline phases in three-flavor quark matter are valid, and expect that the relative favorability of the 2Cube45z and CubeX structures and the qualitative size of their condensation energy are trustworthy, we do not expect quantitative reliability of our results. There is therefore strong motivation to analyze crystalline color superconducting



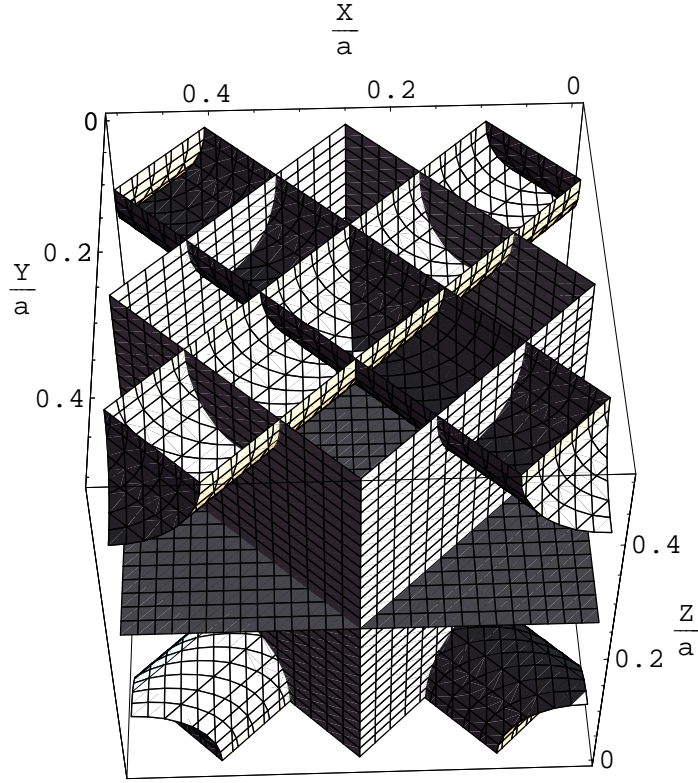


FIG. 8: The CubeX crystal structure of Eq. (90). The figure extends from 0 to  $a=2$  in the  $x, y$  and  $z$  directions. Both  $\psi_2(\mathbf{r})$  and  $\psi_3(\mathbf{r})$  vanish at the horizontal plane.  $\psi_2(\mathbf{r})$  vanishes on the darker vertical planes, and  $\psi_3(\mathbf{r})$  vanishes on the lighter vertical planes. On the upper (lower) dark cylinders and the lower (upper) two small corners of dark cylinders,  $\psi_2(\mathbf{r}) = +3/3$  ( $\psi_2(\mathbf{r}) = -3/3$ ). On the upper (lower) lighter cylinders and the lower (upper) two small corners of lighter cylinders,  $\psi_3(\mathbf{r}) = -3/3$  ( $\psi_3(\mathbf{r}) = +3/3$ ). Note that the largest value of  $j_1(\mathbf{r})$  is 4, occurring along lines at the centers of the cylinders. The lattice spacing is  $a$  when one takes into account the signs of the condensates; if one looks only at  $j_1(\mathbf{r})$ , the lattice spacing is  $a=2$ .  $a$  is given in (88). In (90) and hence in this figure, we have made a particular choice for the relative position of  $\psi_3(\mathbf{r})$  versus  $\psi_2(\mathbf{r})$ . We show in Appendix B that one can be translated relative to the other with no cost in free energy.

quark matter with these two crystal structures without making a Ginzburg-Landau approximation. It will be very interesting to see whether the Ginzburg-Landau approximation underestimates and the condensation energy for the crystalline phases with CubeX and 2Cube45z crystal structures, as it does for the much simpler 2PW structure (in which  $\psi_2(\mathbf{r})$  and  $\psi_3(\mathbf{r})$  are each single plane waves) [41].

Even prior to having a beyond-Ginzburg-Landau analysis available, having an ansatz (actually, two ansätze) for the crystal structure and a good qualitative guide to the scale of  $\psi_2$  and  $\psi_3$  should allow significant progress toward the calculation of astrophysically relevant observables. For example, it would be interesting to evaluate the effects of a

crystalline color superconducting core on the rate at which a neutron star cools by neutrino emission. The specific heat of crystalline color superconducting quark matter is linear with  $T$  because of the presence of gapless quark excitations at the boundaries of the regions in momentum space where there are unpaired quarks [37]. Calculating the heat capacity of the CubeX and 2Cube45z structures should therefore yield only quantitative changes relative to that for unpaired quark matter, unlike in the gCFL case where the heat capacity is parametrically enhanced [16]. The neutrino emissivity should turn out to be significantly suppressed relative to that in unpaired quark matter. The evaluation of the phase space for direct URCA neutrino emission from

the CubeX and 2Cube45z phases will be a nontrivial calculation, given that thermally excited gapless quarks occur only on patches of the Fermi surfaces, separated by the (many) pairing rings. (The direct URCA processes  $u + e \rightarrow s + \bar{u}$  and  $s \rightarrow u + e + \bar{s}$  require  $s$ ,  $u$  and  $e$  to all be within  $T$  of a place in momentum space where they are gapless and at the same time to have  $p_u + p_e = p_s$  to within  $T$ . Here,  $T \sim 10^8$  keV is very small compared to all the scales relevant to the description of the crystalline phase itself.)

Beginning with Ref. [30], one of the motivations for the study of crystalline color superconducting quark matter has been the possibility that, if present within the core of a compact star, it could provide a region within which rotational vortices are pinned and hence a locus for the origin of (some) pulsar glitches. Or, the presence of crystalline quark matter within neutron stars could be ruled out if it predicts glitch phenomenology in qualitative disagreement with that observed.

There are two key microphysical properties of crystalline quark matter that must be estimated before glitch phenomenology can be addressed. The first is the pinning force. Estimating this will require analyzing how the CubeX and 2Cube45z respond when rotated. We expect vortices to form, and expect the vortices to be pinned at the intersections of the nodal planes at which condensates vanish. Analyzing the vortices in three-avor crystalline phases will be nontrivial. One complication is that because baryon number current can be carried by gradients in the phase of either the hsu crystalline condensate or the hdi condensate or both, and the most favorable vortex or vortices that form upon rotating the CubeX and 2Cube45z phases will have to be determined. Another complication arises because the vortex core size,  $l = \lambda$ , is only a factor of three to four smaller than the lattice spacing  $a$ . This means that the vortices cannot be thought of as pinned by an unchanged crystal; the vortices themselves will qualitatively deform the crystalline condensate in their vicinity.

The second microphysical quantity that is required is the shear modulus of the crystal. After all, if vortices are well-pinned but the crystalline condensate can easily deform under shear stress, the vortices will be able to move regardless of the pinning force. Glitches occur if vortices are pinned and immobile while the spinning pulsar's angular velocity slows over years, with the glitch being triggered

by the catastrophic unpinning and motion of long-immobile vortices. In order to immobilize vortices, and hence make glitches a possibility, both the pinning force and the shear modulus must be sufficient. The shear modulus can be related to the coefficients in the low energy effective theory that describes the phonon modes of the crystal [32, 51, 52]. This effective theory has been analyzed, with its coefficients calculated, for the two-avor crystalline color superconductor with face-centered cubic symmetry [52]. Extending this analysis to three-avor crystalline color superconducting phases with the 2Cube45z and CubeX crystal structures is a priority for future work.

Now that we have two well-motivated candidates for the favored crystal structure of the three-avor crystalline color superconducting phase of cold quark matter, favorable over a very wide range of intermediate densities, the challenge becomes calculating the shear modulus and the pinning force exerted on rotational vortices in these structures. These are the prerequisites to determining whether observations of pulsar glitches can be used to rule out (or in) the presence of quark matter in the crystalline color superconducting phase within compact stars.

#### Acknowledgments

We thank K. Fukushima, M. Mannarelli and A. Schmitt for useful discussions. We acknowledge the hospitality of the Nuclear Theory Group at LBNL. This research was supported in part by the Office of Nuclear Physics of the Office of Science of the U.S. Department of Energy under contract #DE-AC02-05CH11231 and cooperative research agreement #DF-FC02-94ER40818.

#### APPENDIX A: NEUTRALITY OF SOLUTIONS WITH $2 = 3$

In Section VIA, we gave a general analysis of the free energy  $\mathcal{F}_2(\mu_2; \mu_3)$ . We showed that if we write  $(\mu_2; \mu_3)$  as  $\frac{1}{2}(\mu_r \cos \theta; \mu_r \sin \theta)$  the free energy takes the form (73), and therefore has extrema only at  $\theta = 0, \pi$  (namely  $\mu_2 = \mu_3 = \mu_r$ ) or  $\theta = \pi/2, 3\pi/2$  (namely a two-avor crystalline phase with only one  $\mu_i$  nonzero). As we have explained in Section IID, in the strict Ginzburg-Landau limit

in which  $\mu_1 = 0$  any solution  $(\mu_2; \mu_3)$  is neutral. (The argument is that choosing  $\mu_e = M_s^2 = 4$ ) as in neutral unpaired quark matter succeeds since, unlike BCS superconductivity, crystalline color superconductivity does not require any modification of the unpaired Fermi momenta prior to pairing and since in the Ginzburg-Landau limit the modifications to number densities due to the pairing itself vanishes.) In this Appendix, we take a small step away from the strict Ginzburg-Landau limit. We assume that  $\mu_r$  is small, but do not work in the limit in which it vanishes. We then show that the only solutions with  $\mu_e = M_s^2 = 4$  and, consequently,  $\mu_2 = \mu_3 = \mu_r = M_s^2 = 8$  which are electrically neutral are those with  $\mu_2 = \mu_3 = \mu_r$ . The two-avor crystalline phases with only one  $\mu_1$  nonzero are not neutral in three-avor quark matter.

The result of this Appendix allows us to neglect solutions which have only one  $\mu_1$  nonzero. This is fortunate, because there are many two-avor crystal structures for which the sextic coefficient is negative, meaning that to sextic order the Ginzburg-Landau potential  $(\mu_2; \mu_3)$  often has runaway directions along the  $\mu_2$  and  $\mu_3$  axes [35]. Furthermore, if the coefficient multiplying  $\sin^2$  in (73) is negative, for example if  $\mu_2$  and  $\mu_3$  are both negative while  $\mu_{32}$  and  $\mu_{322}$  are both positive as is the case for both the Cubex and the 2Cube45z crystal structures on which we focus, then the extremum of  $(\mu_2; \mu_3)$  that we find with  $\mu_2 = \mu_3$  appears to be a local maximum with respect to variation of  $\mu_2$  away from  $\mu_2 = 4$  while keeping  $\mu_e$  fixed. We show in this Appendix that upon fixing  $\mu_e = M_s^2 = 4$  any solution with  $\mu_2 \neq \mu_3$  is not neutral. For this reason, all these complications can be neglected, and we are correct to focus only on solutions with  $\mu_2 = \mu_3$ .

The more formal way to proceed would be to define an  $\mu_{\text{neutral}}(\mu_2; \mu_3)$ , obtained by varying  $\mu_e$  (and  $\mu_3$  and  $\mu_8$  too) at a given value of the  $\mu_i$ 's in order to obtain neutrality, and then finding  $\mu_2$  and  $\mu_3$  that minimize  $\mu_{\text{neutral}}(\mu_2; \mu_3)$ . We have done a partial version of this investigation in a few cases and have found that, as expected,  $\mu_{\text{neutral}}$  does have a minimum with  $\mu_e$  very close to  $M_s^2 = 4$  and  $\mu_2$  very close to  $\mu_3$ . A full exploration in this vein requires evaluating the Ginzburg-Landau coefficients without assuming  $\mu_2 = \mu_3$  and, more challenging, requires reformulating our analysis to include nonzero  $\mu_3$  and  $\mu_8$ . We have not attempted the latter, and it is in this sense that our preliminary investigation referred to above was "partial".

We leave this to future work, and turn now to the promised derivation of the neutrality of solutions with  $\mu_2 = \mu_3$  and  $\mu_e = M_s^2 = 4$ .

We shall only consider crystal structures for which  $f\hat{q}_2g$  and  $f\hat{q}_3g$  are exchange symmetric, as this is the symmetry that allows the free energy to have extrema along the line  $\mu_2 = \mu_3$ . (Recall that by exchange symmetry we mean that there is a sequence of rigid rotations and reflections which when applied to all the vectors in  $f\hat{q}_2g$  and  $f\hat{q}_3g$  together has the effect of exchanging  $f\hat{q}_2g$  and  $f\hat{q}_3g$ .) Because we wish to evaluate  $\mathcal{G} = \mathcal{G}_e$  at  $\mu_e = M_s^2 = 4$ , we must restore  $\mu_e$  to our expression for the free energy, rather than setting it to  $M_s^2 = 4$  from the beginning. Recall from (28) that  $\mu_{\text{crystalline}}$  is the sum of the free energy for unpaired quark matter, which we know satisfies  $\mathcal{G}_{\text{unpaired}} = \mathcal{G}_e = 0$  at  $\mu_e = M_s^2 = 4$ , and  $(\mu_2; \mu_3)$ . Upon restoring the  $\mu_e$ -dependence, the latter is given by

$$\begin{aligned}
 (\mu_e; \mu_2; \mu_3) = & \\
 & \frac{\mu_2^2}{2} P(\mu_2) + \frac{\mu_3^2}{2} P(\mu_3) \\
 & + \frac{1}{2} \frac{\mu_2^4}{2} + \frac{1}{2} \frac{\mu_3^4}{3} + \frac{1}{3} \mu_2^2 \mu_3^2 \\
 & + \frac{1}{3} \frac{\mu_2^6}{2} + \frac{1}{3} \frac{\mu_3^6}{3} + \mu_{233} (\mu_2; \mu_3) \mu_2^2 \mu_3^4 \\
 & ! \# \\
 & + \mu_{322} (\mu_2; \mu_3) \mu_2^2 \mu_3^4 ;
 \end{aligned} \tag{A1}$$

where  $\mu_2$  and  $\mu_3$  can no longer be taken to be equal, as they are given by

$$\begin{aligned}
 \mu_3 &= \frac{e}{2} \\
 \mu_2 &= \frac{M_s^2}{4} - \frac{e}{2} ;
 \end{aligned} \tag{A2}$$

which in particular means that

$$\frac{\mathcal{G}_{\mu_3}}{\mathcal{G}_e} = \frac{\mathcal{G}_{\mu_2}}{\mathcal{G}_e} = \frac{1}{2} ; \tag{A3}$$

Because  $f\hat{q}_2g$  and  $f\hat{q}_3g$  are exchange symmetric,  $\mu_2 = \mu_3$  and  $\mu_2 = \mu_3$ . Because  $\mu_2 \neq \mu_3$ , however, the coefficients  $\mu_{322}$  and  $\mu_{233}$  are not equal and, furthermore, their  $(\mu_2; \mu_3)$ -dependence cannot be factored out as in (57) or

(71). The coefficient  $\epsilon_{322}$  depends on  $\epsilon_2$  and  $\epsilon_3$  through its dependence on  $K_{\text{udusus}}$ :  $\epsilon_{322} = (3=2) K_{\text{udusus}}(q_3^b; q_3^b; q_2^d; q_2^e; q_2^f; q_2^a)$ .  $K_{\text{udusus}}$  is given in (67). Note that its dependence on  $\epsilon_2$  and  $\epsilon_3$  comes via  $q_2 = \epsilon_2 \hat{q}_2$  and  $q_3 = \epsilon_3 \hat{q}_3$  in addition to the explicit dependence visible in (67). Similarly

$\epsilon_{233} = (3=2) K_{\text{usudud}}(q_2^b; q_2^b; q_3^d; q_3^e; q_3^f; q_3^a)$  where  $K_{\text{usudud}}$  has the same form as (67) except that  $\epsilon_2$  and  $\epsilon_3$  are interchanged. Using the definitions (57) and (71), one can confirm that (A1) reduces to (72) if we take  $\epsilon_2 = \epsilon_3$  and hence  $\epsilon_{322} = \epsilon_{233}$ .

We now differentiate given in (A1) with respect to  $\epsilon_e$ , noting (A3), obtaining

$$\begin{aligned} \frac{\partial}{\partial \epsilon_e} = & \frac{\partial}{\partial \epsilon_2} \frac{d}{d \epsilon_e} \epsilon_2 + \frac{\partial}{\partial \epsilon_3} \frac{d}{d \epsilon_e} \epsilon_3 + \frac{1}{2} P \frac{d(\epsilon_3)}{d \epsilon_3} \epsilon_2^2 + P \frac{d(\epsilon_2)}{d \epsilon_2} \epsilon_2^2 + \frac{1}{2} \epsilon_3^4 - \frac{1}{3} \epsilon_3^4 \\ & + \frac{1}{2} \frac{1}{\epsilon_2^2} \frac{1}{\epsilon_3} \epsilon_3^2 \epsilon_2^2 + \frac{4}{3} \frac{1}{\epsilon_2^5} \epsilon_2^6 + \frac{4}{3} \frac{1}{\epsilon_3^5} \epsilon_3^6 \\ & + \frac{1}{3} \frac{\partial \epsilon_{233}(\epsilon_2; \epsilon_3)}{\partial \epsilon_3} \epsilon_2^2 \epsilon_3^4 + \frac{1}{3} \frac{\partial \epsilon_{322}(\epsilon_2; \epsilon_3)}{\partial \epsilon_3} \epsilon_2^4 \epsilon_3^2 + \frac{\partial \epsilon_{322}(\epsilon_2; \epsilon_3)}{\partial \epsilon_2} \epsilon_2^4 \epsilon_3^2 : \end{aligned} \quad (\text{A } 4)$$

We shall only evaluate  $\partial/\partial \epsilon_e$  at values of  $\epsilon_2$  and  $\epsilon_3$  which are solutions to the gap equations  $\partial/\partial \epsilon_2 = 0$  and  $\partial/\partial \epsilon_3 = 0$ , meaning that the first two terms in (A4) vanish. Furthermore, we shall only evaluate  $\partial/\partial \epsilon_e$  at  $\epsilon_e = M_s^2/4$ , where  $\epsilon_2 = \epsilon_3 = \epsilon_{\text{min}}$ , and at solutions for which  $\epsilon_2 = \epsilon_3$ . Under these circumstances, the terms involving  $\epsilon_2^6$ ,  $\epsilon_3^6$  and  $\epsilon_2^4 \epsilon_3^2$  vanish and (A4) becomes

$$\frac{\partial}{\partial \epsilon_e} \bigg|_{\epsilon_e = \frac{M_s^2}{4}; \epsilon_2 = \epsilon_3 = \epsilon_{\text{min}}} = \frac{1}{3} \frac{\partial \epsilon_{233}}{\partial \epsilon_3} \bigg|_{\epsilon_2 = \epsilon_3 = \epsilon_{\text{min}}} + \frac{\partial \epsilon_{322}}{\partial \epsilon_3} \bigg|_{\epsilon_2 = \epsilon_3 = \epsilon_{\text{min}}} + \frac{\partial \epsilon_{322}}{\partial \epsilon_2} \bigg|_{\epsilon_2 = \epsilon_3 = \epsilon_{\text{min}}} \quad (\text{A } 5)$$

We argue that this vanishes as follows. Consider a particular term that contributes to  $\epsilon_{322} = \epsilon_{2,2}$ ,  $\epsilon_{K_{\text{udusus}}}(q_3^b; q_3^b; q_2^d; q_2^e; q_2^f; q_2^a) = \epsilon_{2,2}$ . This is a complicated integral of a function which depends on the unit momentum vectors  $(\hat{q}_3^b; \hat{q}_2^d; \hat{q}_2^e; \hat{q}_2^f; \hat{q}_2^a)$  and on  $\epsilon_2$  and  $\epsilon_3$ . From rotational invariance, we know that the value of the integral can depend on the relative orientation of the unit momentum vectors and on  $\epsilon_2$  and  $\epsilon_3$  but must be independent of common rotations of all the unit vectors. Now, all the crystal structures that we consider are exchange symmetric, meaning that for every quintuple of unit momentum vectors,  $(\hat{q}_3^b; \hat{q}_2^d; \hat{q}_2^e; \hat{q}_2^f; \hat{q}_2^a)$  with the first chosen from  $f_{q_3g}$  and the last four chosen from  $f_{q_2g}$  there exists a quintuple  $(\hat{q}_2^b; \hat{q}_3^d; \hat{q}_3^e; \hat{q}_3^f; \hat{q}_3^a)$  with the first chosen from  $f_{q_2g}$  and the last four chosen from  $f_{q_3g}$  such that the unit vectors in each of these two quintuples have the same relative orientation among themselves. This means that for

every term  $\epsilon_{K_{\text{udusus}}}(q_3^b; q_3^b; q_2^d; q_2^e; q_2^f; q_2^a) = \epsilon_{2,2}$  occurring in  $\epsilon_{322} = \epsilon_{2,2}$ , there is a corresponding term  $\epsilon_{K_{\text{usudud}}}(q_2^b; q_2^b; q_3^d; q_3^e; q_3^f; q_3^a) = \epsilon_{3,3}$  occurring in  $\epsilon_{233} = \epsilon_{3,3}$  such that  $\epsilon_{K_{\text{usudud}}}(q_2^b; q_2^b; q_3^d; q_3^e; q_3^f; q_3^a) = \epsilon_{3,3}$  is related to  $\epsilon_{K_{\text{udusus}}}(q_3^b; q_3^b; q_2^d; q_2^e; q_2^f; q_2^a) = \epsilon_{2,2}$  by the interchange of  $\epsilon_2$  and  $\epsilon_3$ . Consequently, for  $\epsilon_2 = \epsilon_3$  the two contributions cancel pair by pair when we evaluate  $\epsilon_{322} = \epsilon_{2,2} - \epsilon_{233} = \epsilon_{3,3}$  or  $\epsilon_{322} = \epsilon_{3,3} - \epsilon_{233} = \epsilon_{2,2}$ . In this way, the right hand side of (A5) vanishes, as we set out to show. We conclude that solutions to the gap equations with  $\epsilon_2 = \epsilon_3$  and  $\epsilon_e = M_s^2/4$  meaning  $\epsilon_2 = \epsilon_3$  are neutral.

It is easy to see that the cancellations required in the proof of neutrality do not occur for solutions with  $\epsilon_2 \neq \epsilon_3$ . For example, following a derivation analogous to that above, we find that a solution with  $\epsilon_2 = 0$  and only  $\epsilon_3$  nonzero is neutral with  $\epsilon_e =$

$M_s^2 = (4)$  only if

$$P \frac{\partial}{\partial \epsilon_3} \left( \frac{\epsilon_3}{3} \right)^{\frac{2}{3}} - \frac{3}{3} \frac{\partial}{\partial \epsilon_3} \left( \frac{\epsilon_3}{3} \right)^{\frac{4}{3}} + \frac{4}{3} \frac{\partial}{\partial \epsilon_3} \left( \frac{\epsilon_3}{3} \right)^{\frac{6}{3}} = 0; \quad (\text{A } 6)$$

a condition which has no reason to be satisfied. The study of solutions with  $\epsilon_2 \neq \epsilon_3$  therefore requires that they be constructed from the beginning with  $\epsilon_2 \neq \epsilon_3$  and with  $\epsilon$  fixed by the neutrality condition. We leave this to future work, focussing in Section VI on solutions with  $\epsilon_2 = \epsilon_3$  which, we have proved here, are neutral.

#### APPENDIX B: TRANSLATING $\mu_{\text{hisi}}$ RELATIVE TO $\mu_{\text{hidi}}$ DOES NOT AVOID REPULSION

We have seen in Section VI that crystal structures in which a vector from  $\text{fq}_2\text{g}$  and a vector from  $\text{fq}_3\text{g}$  make a 180° angle are strongly disfavored, with infinite quartic and sextic Ginzburg-Landau coefficients  $\beta_{32}$  and  $\beta_{322}$ . Suppose we consider a structure like that in which  $\text{fq}_2\text{g}$  and  $\text{fq}_3\text{g}$  are coincident cubes, a disastrous choice. The way that we have improved upon this disastrous choice in Section VID is to rotate one cube relative to the other. Indeed, if we choose a 45° rotation about an axis perpendicular to a face of the cube, we obtain the 2Cube45z structure which is one of the two crystal structures that

we find to be most favorable. In this Appendix, we ask whether we can instead avoid the infinite free energy cost of antipodal pairs by translating the hidi condensate relative to the hisi condensate in position space, rather than rotating it. We find that the answer is no, and furthermore show that the Ginzburg-Landau free energy that we have evaluated does not change if the hidi condensate is translated relative to the hisi condensate.

Corresponding to each  $\text{fq}_I\text{g}$  in momentum space we get a function  $\phi_I(\mathbf{r})$  in position space which varies as  $\phi_I(\mathbf{r}) = \sum_{\mathbf{q}_I^a} e^{2i\mathbf{q}_I^a \cdot \mathbf{r}}$ . To analyze the effects of translating  $\phi_2(\mathbf{r})$  relative to  $\phi_3(\mathbf{r})$ , it is helpful to restore the notation of (40) with  $(\mathbf{q}_I^a)$  representing the gap parameter corresponding to the momentum component  $\mathbf{q}_I^a$ .  $\phi_2(\mathbf{r})$  or  $\phi_3(\mathbf{r})$  can then be written as

$$\phi_I(\mathbf{r}) = \sum_{\mathbf{q}_I^a} (\mathbf{q}_I^a) e^{2i\mathbf{q}_I^a \cdot \mathbf{r}}; \quad (\text{B } 1)$$

Translating  $\phi_2(\mathbf{r})$  in the  $\hat{n}$  direction by a distance  $s$  corresponds to the transformation  $\phi_2(\mathbf{r}) \rightarrow \phi_2(\mathbf{r} + s\hat{n})$  which multiplies each  $(\mathbf{q}_2^a)$  in the sum in (B1) by a different phase factor  $\exp[2is\mathbf{q}_2^a \cdot \hat{n}]$ . This is not just an (irrelevant) overall phase multiplying  $\phi_2(\mathbf{r})$  because it depends on the momentum component. The gap equation for the  $\phi_2$  components, as in (40), is now given by

$$\begin{aligned} (\mathbf{q}_2^a) e^{2is\mathbf{q}_2^a \cdot \hat{n}} = & \frac{2}{2} \sum_{\mathbf{q}_2^b, \mathbf{q}_2^c, \mathbf{q}_2^d} (\mathbf{q}_2^a) e^{2is\mathbf{q}_2^a \cdot \hat{n}} J_{3131}(\mathbf{q}_2^b; \mathbf{q}_2^c; \mathbf{q}_2^d; \mathbf{q}_2^a) \\ & + \sum_{\mathbf{q}_2^b, \mathbf{q}_2^c, \mathbf{q}_2^d} (\mathbf{q}_2^b) (\mathbf{q}_2^c) (\mathbf{q}_2^d) e^{2is(\mathbf{q}_2^b + \mathbf{q}_2^c + \mathbf{q}_2^d) \cdot \hat{n}} J_{3131}(\mathbf{q}_2^b; \mathbf{q}_2^c; \mathbf{q}_2^d; \mathbf{q}_2^a) \\ & + \frac{1}{2} \sum_{\mathbf{q}_3^b, \mathbf{q}_3^c, \mathbf{q}_2^d} (\mathbf{q}_3^b) (\mathbf{q}_3^c) (\mathbf{q}_2^d) e^{2is\mathbf{q}_2^d \cdot \hat{n}} J_{1213}(\mathbf{q}_3^b; \mathbf{q}_3^c; \mathbf{q}_2^d; \mathbf{q}_2^a) \end{aligned} \quad (\text{B } 2)$$

where we have worked only to cubic order. Using  $\mathbf{q}_2^b + \mathbf{q}_2^c + \mathbf{q}_2^d = \mathbf{q}_2^a$  we conclude that the phase factor in front of the  $J_{3131}(\mathbf{q}_2^b; \mathbf{q}_2^c; \mathbf{q}_2^d; \mathbf{q}_2^a)$  term is simply  $\exp[2is(\mathbf{q}_2^a) \cdot \hat{n}]$ . In addition, we saw that for  $\mathbf{q}_3^b + \mathbf{q}_3^c + \mathbf{q}_2^d = \mathbf{q}_2^a$  to hold we need to have  $\mathbf{q}_3^b = \mathbf{q}_3^c$  and  $\mathbf{q}_2^d = \mathbf{q}_2^a$ . This makes the phase factor in front

of  $J_{1213}(\mathbf{q}_3^b; \mathbf{q}_3^c; \mathbf{q}_2^d; \mathbf{q}_2^a)$  also  $\exp[2is(\mathbf{q}_2^a) \cdot \hat{n}]$ . We conclude that (up to cubic order) the gap equation for each  $(\mathbf{q}_2^a)$  simply picks up an overall phase. The same is true for the gap equation for each  $(\mathbf{q}_3^a)$ . We therefore conclude that the free energy is unchanged up to quartic order when  $\phi_2(\mathbf{r})$  is translated relative



to  $\phi_3(r)$ . This guarantees that such a translation cannot alleviate the large  $\phi_2$  arising from antipodal (or near antipodal) pairs of momenta occurring in  $f_{q_2g}$  and  $f_{q_3g}$ . This argument can easily be ex-

tended to include the sextic terms in the free energy; they too are unchanged when  $\phi_2(r)$  is translated relative to  $\phi_3(r)$ .

- 
- [1] For reviews, see K. Rajagopal and F. W. Ilczek, *arXiv hep-ph/0011333*; M. G. Alford, *Ann. Rev. Nucl. Part. Sci.* 51, 131 (2001) [*arXiv hep-ph/0102047*]; G. Nardulli, *Riv. Nuovo Cim.* 25N 3, 1 (2002) [*arXiv hep-ph/0202037*]; S. Reddy, *Acta Phys. Polon. B* 33, 4101 (2002) [*arXiv nucl-th/0211045*]; T. Schafer, *arXiv hep-ph/0304281*; D. H. Rischke, *Prog. Part. Nucl. Phys.* 52, 197 (2004) [*arXiv nucl-th/0305030*]; M. Alford, *Prog. Theor. Phys. Suppl.* 153, 1 (2004) [*arXiv nucl-th/0312007*]; M. Buballa, *Phys. Rept.* 407, 205 (2005) [*arXiv hep-ph/0402234*]; H. C. Ren, *arXiv hep-ph/0404074*; I. Shovkovy, *arXiv nucl-th/0410091*; T. Schafer, *arXiv hep-ph/0509068*; T. Schafer, *arXiv hep-ph/0602067*.
- [2] J. Bardeen, L. N. Cooper, and J. R. Schrieffer, *Phys. Rev.* 108, 1175 (1957).
- [3] M. Iwasaki and T. Iwado, *Phys. Lett. B* 350, 163 (1995). T. Schafer, *Phys. Rev. D* 62, 094007 (2000) [*arXiv hep-ph/0006034*]; M. Buballa, J. Hosek and M. Oertel, *Phys. Rev. Lett.* 90, 182002 (2003) [*arXiv hep-ph/0204275*]; A. Schmitt, Q. Wang and D. H. Rischke, *Phys. Rev. D* 66, 114010 (2002) [*arXiv nucl-th/0209050*]; M. G. Alford, J. A. Bowers, J. M. Cheyne and G. A. Cowan, *Phys. Rev. D* 67, 054018 (2003) [*arXiv hep-ph/0210106*]; A. Schmitt, *Phys. Rev. D* 71, 054016 (2005) [*arXiv nucl-th/0412033*]; M. G. Alford and G. A. Cowan, *J. Phys. G* 32, 511 (2006) [*arXiv hep-ph/0512104*].
- [4] M. G. Alford, K. Rajagopal and F. W. Ilczek, *Phys. Lett. B* 422, 247 (1998) [*arXiv hep-ph/9711395*].
- [5] M. G. Alford, K. Rajagopal and F. W. Ilczek, *Nucl. Phys. B* 537, 443 (1999) [*arXiv hep-ph/9804403*].
- [6] M. Alford and K. Rajagopal, *JHEP* 0206, 031 (2002) [*arXiv hep-ph/0204001*].
- [7] K. Iida and G. Baym, *Phys. Rev. D* 63, 074018 (2001) [Erratum-*ibid.* *D* 66, 059903 (2002)] [*arXiv hep-ph/0011229*].
- [8] Stable bulk matter must be neutral under all gauged charges, whether they are spontaneously broken or not. In the case of the electromagnetic gauge symmetry, this simply requires zero charge density. In the case of the color gauge symmetry, bulk matter must in fact be a color singlet, which is a more restrictive condition than mere color neutrality. However, the free energy cost of projecting a color neutral state onto a color singlet state falls rapidly with volume, as long as we are considering volumes larger than the size of a Cooper pair. Given that if quark matter occurs within the core of a neutron star the relevant volumes will be of order cubic kilometers, whereas Cooper pairs have sizes of order fm, it is more than sufficient to consider only the consequences of enforcing color neutrality. See P. Amore, M. C. Birse, J. A. McGovern and N. R. Walet, *Phys. Rev. D* 65, 074005 (2002) [*arXiv hep-ph/0110267*].
- [9] A. W. Steiner, S. Reddy and M. Prakash, *Phys. Rev. D* 66, 094007 (2002) [*arXiv hep-ph/0205201*].
- [10] M. Huang, P. f. Zhuang and W. q. Chao, *Phys. Rev. D* 67, 065015 (2003) [*arXiv hep-ph/0207008*]; F. Neumann, M. Buballa and M. Oertel, *Nucl. Phys. A* 714, 481 (2003) [*arXiv hep-ph/0210078*].
- [11] M. Alford, C. Kouvaris and K. Rajagopal, *Phys. Rev. Lett.* 92, 222001 (2004) [*arXiv hep-ph/0311286*].
- [12] M. Alford, C. Kouvaris and K. Rajagopal, *Phys. Rev. D* 71, 054009 (2005) [*arXiv hep-ph/0406137*].
- [13] M. Alford, C. Kouvaris and K. Rajagopal, *arXiv hep-ph/0407257*.
- [14] S. B. Ruster, I. A. Shovkovy and D. H. Rischke, *Nucl. Phys. A* 743, 127 (2004) [*arXiv hep-ph/0405170*].
- [15] K. Fukushima, C. Kouvaris and K. Rajagopal, *Phys. Rev. D* 71, 034002 (2005) [*arXiv hep-ph/0408322*].
- [16] M. Alford, P. Jotwani, C. Kouvaris, J. Kundu and K. Rajagopal, *Phys. Rev. D* 71, 114011 (2005) [*arXiv astro-ph/0411560*].
- [17] H. Abuki, M. Kitazawa and T. Kunihito, *Phys. Lett. B* 615, 102 (2005) [*arXiv hep-ph/0412382*].
- [18] S. B. Ruster, V. W. Gerth, M. Buballa, I. A. Shovkovy and D. H. Rischke, *Phys. Rev. D* 72, 034004 (2005) [*arXiv hep-ph/0503184*].
- [19] I. Shovkovy and M. Huang, *Phys. Lett. B* 564, 205 (2003) [*arXiv hep-ph/0302142*]; M. Huang and I. Shovkovy, *Nucl. Phys. A* 729, 835 (2003) [*arXiv hep-ph/0307273*].
- [20] E. Gubankova, W. V. Liu and F. W. Ilczek, *Phys. Rev. Lett.* 91, 032001 (2003) [*arXiv hep-ph/0304016*].
- [21] M. Huang and I. A. Shovkovy, *Phys. Rev. D* 70, 051501 (2004) [*arXiv hep-ph/0407049*]; M. Huang and I. A. Shovkovy, *Phys. Rev. D* 70, 094030 (2004) [*arXiv hep-ph/0408268*]; I. Giannakis and H. C. Ren, *Phys. Lett. B* 611, 137 (2005)

- [arXiv:hep-ph/0412015]; M. A. Lford and Q. h. W ang, J. Phys. G 31, 719 (2005) [arXiv:hep-ph/0501078]; M. Huang, Phys. Rev. D 73, 045007 (2006) [arXiv:hep-ph/0504235]; E. V. Gorbar, M. Hashimoto and V. A. Miransky, Phys. Lett. B 632, 305 (2006) [arXiv:hep-ph/0507303]; E. V. Gorbar, M. Hashimoto, V. A. Miransky and I. A. Shovkovy, arXiv:hep-ph/0602251; K. Iida and K. Fukushima, arXiv:hep-ph/0603179.
- [22] R. Casalbuoni, R. Gatto, M. Mannarelli, G. Nardulli and M. Ruggieri, Phys. Lett. B 605, 362 (2005) [Erratum-ibid. B 615, 297 (2005)] [arXiv:hep-ph/0410401]; K. Fukushima, Phys. Rev. D 72, 074002 (2005) [arXiv:hep-ph/0506080].
- [23] K. Fukushima, arXiv:hep-ph/0603216.
- [24] P. F. Bedaque, H. Caldas and G. Rupak, Phys. Rev. Lett. 91, 247002 (2003) [arXiv:cond-mat/0306694]; M. M. Forbes, E. Gubankova, W. V. Liu and F. Wilczek, Phys. Rev. Lett. 94, 017001 (2005) [arXiv:hep-ph/0405059]; S. Reddy and G. Rupak, Phys. Rev. C 71, 025201 (2005) [arXiv:nucl-th/0405054]; J. Carlson and S. Reddy, Phys. Rev. Lett. 95, 060401 (2005) [arXiv:cond-mat/0503256].
- [25] M. W. Zwiernik, A. Schirotzek, C. H. Schunck, and W. Ketterle, Science 311, 492 (2006) [arXiv:cond-mat/0511197].
- [26] G. B. Partridge, W. Li, R. I. Kamar, Y.-a. Liao, and R. G. Hulet, Science 311, 503 (2006) [arXiv:cond-mat/0511752].
- [27] D. Bailin and A. Love, Phys. Rept. 107, 325 (1984).
- [28] R. Rapp, T. Schafer, E. V. Shuryak and M. Velkovsky, Phys. Rev. Lett. 81, 53 (1998) [arXiv:hep-ph/9711396].
- [29] K. Rajagopal and A. Schmitt, Phys. Rev. D 73, 045003 (2006) [arXiv:hep-ph/0512043].
- [30] M. G. A. Lford, J. A. Bowers and K. Rajagopal, Phys. Rev. D 63, 074016 (2001) [arXiv:hep-ph/0008208].
- [31] J. A. Bowers, J. Kundu, K. Rajagopal and E. Shuster, Phys. Rev. D 64, 014024 (2001) [arXiv:hep-ph/0101067].
- [32] R. Casalbuoni, R. Gatto, M. Mannarelli and G. Nardulli, Phys. Lett. B 511, 218 (2001) [arXiv:hep-ph/0101326].
- [33] A. K. Leibovich, K. Rajagopal and E. Shuster, Phys. Rev. D 64, 094005 (2001) [arXiv:hep-ph/0104073].
- [34] J. Kundu and K. Rajagopal, Phys. Rev. D 65, 094022 (2002) [arXiv:hep-ph/0112206].
- [35] J. A. Bowers and K. Rajagopal, Phys. Rev. D 66, 065002 (2002) [arXiv:hep-ph/0204079].
- [36] R. Casalbuoni and G. Nardulli, Rev. Mod. Phys. 76, 320 (2004) [arXiv:hep-ph/0305069].
- [37] R. Casalbuoni, R. Gatto, M. Mannarelli, G. Nardulli, M. Ruggieri and S. Stramaglia, Phys. Lett. B 575, 181 (2003) [Erratum-ibid. B 582, 279 (2004)] [arXiv:hep-ph/0307335].
- [38] R. Casalbuoni, M. Ciminale, M. Mannarelli, G. Nardulli, M. Ruggieri and R. Gatto, Phys. Rev. D 70, 054004 (2004) [arXiv:hep-ph/0404090].
- [39] R. Casalbuoni, R. Gatto, N. Ippolito, G. Nardulli and M. Ruggieri, Phys. Lett. B 627, 89 (2005) [arXiv:hep-ph/0507247].
- [40] M. Ciminale, G. Nardulli, M. Ruggieri and R. Gatto, Phys. Lett. B 636, 317 (2006) [arXiv:hep-ph/0602180].
- [41] M. Mannarelli, K. Rajagopal and R. Sharma, arXiv:hep-ph/0603076.
- [42] A. I. Larkin and Yu. N. Ovchinnikov, Zh. Eksp. Teor. Fiz. 47, 1136 (1964) [Sov. Phys. JETP 20, 762 (1965)]; P. Fulde and R. A. Ferrell, Phys. Rev. 135, A550 (1964); S. Takada and T. Izuyama, Prog. Theor. Phys. 41, 635 (1969).
- [43] P. F. Bedaque and T. Schafer, Nucl. Phys. A 697, 802 (2002) [arXiv:hep-ph/0105150]; D. B. Kaplan and S. Reddy, Phys. Rev. D 65, 054042 (2002) [arXiv:hep-ph/0107265]; A. Kryjevski, D. B. Kaplan and T. Schafer, Phys. Rev. D 71, 034004 (2005) [arXiv:hep-ph/0404290].
- [44] A. Kryjevski and T. Schafer, Phys. Lett. B 606, 52 (2005) [arXiv:hep-ph/0407329]; A. Kryjevski and D. Yamada, Phys. Rev. D 71, 014011 (2005) [arXiv:hep-ph/0407350]; M. Buballa, Phys. Lett. B 609, 57 (2005) [arXiv:hep-ph/0410397]; M. M. Forbes, Phys. Rev. D 72, 094032 (2005) [arXiv:hep-ph/0411001].
- [45] A. Kryjevski, arXiv:hep-ph/0508180; T. Schafer, Phys. Rev. Lett. 96, 012305 (2006) [arXiv:hep-ph/0508190].
- [46] A. Gerhold and T. Schafer, arXiv:hep-ph/0603257.
- [47] A. Gerhold and A. Rebhan, Phys. Rev. D 68, 011502 (2003) [arXiv:hep-ph/0305108]; A. Kryjevski, Phys. Rev. D 68, 074008 (2003) [arXiv:hep-ph/0305173]; A. Gerhold, Phys. Rev. D 71, 014039 (2005) [arXiv:hep-ph/0411086]; D. D. Dietrich and D. H. Rischke, Prog. Part. Nucl. Phys. 53, 305 (2004) [arXiv:nucl-th/0312044].
- [48] K. Rajagopal and F. Wilczek, Phys. Rev. Lett. 86, 3492 (2001) [arXiv:hep-ph/0012039].
- [49] T. Schafer, Nucl. Phys. B 575, 269 (2000) [arXiv:hep-ph/9909574].
- [50] S. Alexander and J. McTague, Phys. Rev. Lett. 41, 705 (1978); for a textbook treatment, see P. M. Chaikin and T. C. Lubensky, Principles of Condensed Matter Physics, (Cambridge University Press, 1995).
- [51] R. Casalbuoni, R. Gatto, M. Mannarelli and G. Nardulli, Phys. Rev. D 66, 014006 (2002) [arXiv:hep-ph/0201059].
- [52] R. Casalbuoni, E. Fabiano, R. Gatto, M. Mannarelli and G. Nardulli, Phys. Rev. D 66, 094006 (2002) [arXiv:hep-ph/0208121].